



1 **The 852/3 CE Mount Churchill eruption: examining the potential**
2 **climatic and societal impacts and the timing of the Medieval**
3 **Climate Anomaly in the North Atlantic Region**

4 Helen Mackay¹, Gill Plunkett², Britta J.L. Jensen³, Thomas J. Aubry⁴, Christophe Corona^{5,6}, Woon
5 Mi Kim^{7,8}, Matthew Toohey⁹, Michael Sigl^{7,8}, Markus Stoffel^{6,10,11}, Kevin J. Anchukaitis¹²,
6 Christoph Raible^{7,8}, Matthew S. M. Bolton³, Joseph G. Manning¹³, Timothy P. Newfield^{14,15},
7 Nicola Di Cosmo¹⁶, Francis Ludlow¹⁷, Conor Kostick¹⁷, Zhen Yang¹⁷, Lisa Coyle McClung²,
8 Matthew Amesbury¹⁸, Alistair Monteath³, Paul D.M. Hughes¹⁹, Pete G. Langdon¹⁹, Dan
9 Charman¹⁸, Robert Booth²⁰, Kimberley L. Davies²¹, Antony Blundell²², and Graeme T. Swindles²³

10

11 ¹Department of Geography, Durham University, Durham, DH1 3LE, UK

12 ²Archaeology & Palaeoecology, School of Natural and Built Environment, Queen's University Belfast, Belfast, BT7
13 INN, UK

14 ³Earth and Atmospheric Sciences, Faculty of Science, University of Alberta, Edmonton, Alberta, T6G 2E3, Canada

15 ⁴Department of Geography, University of Cambridge, UK; Sidney Sussex College, Cambridge, CB2 3HU, UK

16 ⁵Université Clermont-Auvergne, Geolab UMR 6042 CNRS, France

17 ⁶Institute for Environmental Sciences, University of Geneva, CH-1205 Geneva, Switzerland

18 ⁷Climate and Environmental Physics, Physics Institute, University of Bern, Bern, CH-3012, Switzerland

19 ⁸Oeschger Centre for Climate Change Research, University of Bern, Bern, CH-3012, Switzerland

20 ⁹Institute of Space and Atmospheric Studies, University of Saskatchewan, Saskatoon, S7N 5E2, Canada

21 ¹⁰Department of Earth Sciences, University of Geneva, CH-1205 Geneva, Switzerland

22 ¹¹Department F.-A. Forel for Environmental and Aquatic Sciences, University of Geneva, CH-1205 Geneva,
23 Switzerland

24 ¹²School of Geography, Development, and Environment and Laboratory of Tree-Ring Research, University of
25 Arizona, Tucson, AZ 85721 USA

26 ¹³Department of History, Yale University, New Haven, 06520, USA

27 ¹⁴Department of History, Georgetown University, Washington, 20057, USA (TN)

28 ¹⁵Department of Biology, Georgetown University, Washington, 20057, USA (TN)

29 ¹⁶Institute for Advanced Study, Princeton, New Jersey, 08540, USA

30 ¹⁷Department of History, and Trinity Centre for Environmental Humanities, Trinity College Dublin, Dublin, D02
31 PN40, Ireland.

32 ¹⁸Geography, College of Life and Environmental Sciences, University of Exeter, EX4 4ST, UK

33 ¹⁹School of Geography and Environmental Science, University of Southampton, SO17 1BJ, UK

34 ²⁰Earth and Environmental Science Department, Lehigh University, Pennsylvania, 18015, USA

35 ²¹Institute for Modelling Socio-Environmental Transitions, Bournemouth University, Bournemouth, BH12 5BB, UK

36 ²²School of Geography, University of Leeds, Leeds, LS2 9JT, UK

37 ²³Geography, School of Natural and Built Environment, Queen's University Belfast, Belfast, BT7 1NN, UK

38 *Correspondence to:* Helen Mackay (helen.mackay@durham.ac.uk)

39



40 Abstract

41 The 852/3 CE eruption of Mount Churchill, Alaska, was one of the largest first millennium volcanic events, with a
42 magnitude of 6.7 (VEI 6) and a tephra volume of 39.4–61.9 km³ (95% confidence). The spatial extent of the ash
43 fallout from this event is considerable and the cryptotephra (White River Ash east; WRAe) extends as far as Finland
44 and Poland. Proximal ecosystem and societal disturbances have been linked with this eruption; however, wider
45 eruption impacts on climate and society are unknown. Greenland ice-core records show that the eruption occurred in
46 winter 852/3 ± 1 CE and that the eruption is associated with a relatively moderate sulfate aerosol loading, but large
47 abundances of volcanic ash and chlorine. Here we assess the potential broader impact of this eruption using
48 palaeoenvironmental reconstructions, historical records and climate model simulations. We also use the fortuitous
49 timing of the 852/3 CE Churchill eruption and its extensively widespread tephra deposition of the White River Ash
50 (east) (WRAe) to examine the climatic expression of the warm Medieval Climate Anomaly period (MCA; ca. 950–
51 1250 CE) from precisely linked peatlands in the North Atlantic region.

52 The reconstructed climate forcing potential of 852/3 CE Churchill eruption is moderate compared with the eruption
53 magnitude, but tree-ring-inferred temperatures report a significant atmospheric cooling of 0.8 °C in summer 853 CE.
54 Modelled climate scenarios also show a cooling in 853 CE, although the average magnitude of cooling is smaller
55 (0.3 °C). The simulated spatial patterns of cooling are generally similar to those generated using the tree-ring-
56 inferred temperature reconstructions. Tree-ring inferred cooling begins prior to the date of the eruption suggesting
57 that natural internal climate variability may have increased the climate system's susceptibility to further cooling.
58 The magnitude of the reconstructed cooling could also suggest that the climate forcing potential of this eruption may
59 be underestimated, thereby highlighting the need for greater insight into, and consideration of, the role of halogens
60 and volcanic ash when estimating eruption climate forcing potential.

61 Precise comparisons of palaeoenvironmental records from peatlands across North America and Europe, facilitated
62 by the presence of the WRAe isochron, reveal no consistent MCA signal. These findings contribute to the growing
63 body of evidence that characterizes the MCA hydroclimate as time-transgressive and heterogeneous, rather than a
64 well-defined climatic period. The presence of the WRAe isochron also demonstrates that no long-term
65 (multidecadal) climatic or societal impacts from the 852/3 CE Churchill eruption were identified beyond areas
66 proximal to the eruption. Historical evidence in Europe for subsistence crises demonstrate a degree of temporal
67 correspondence on interannual timescales, but similar events were reported outside of the eruption period and were
68 common in the 9th century. The 852/3 CE Churchill eruption exemplifies the difficulties of identifying and
69 confirming volcanic impacts for a single eruption, even when it is precisely dated.

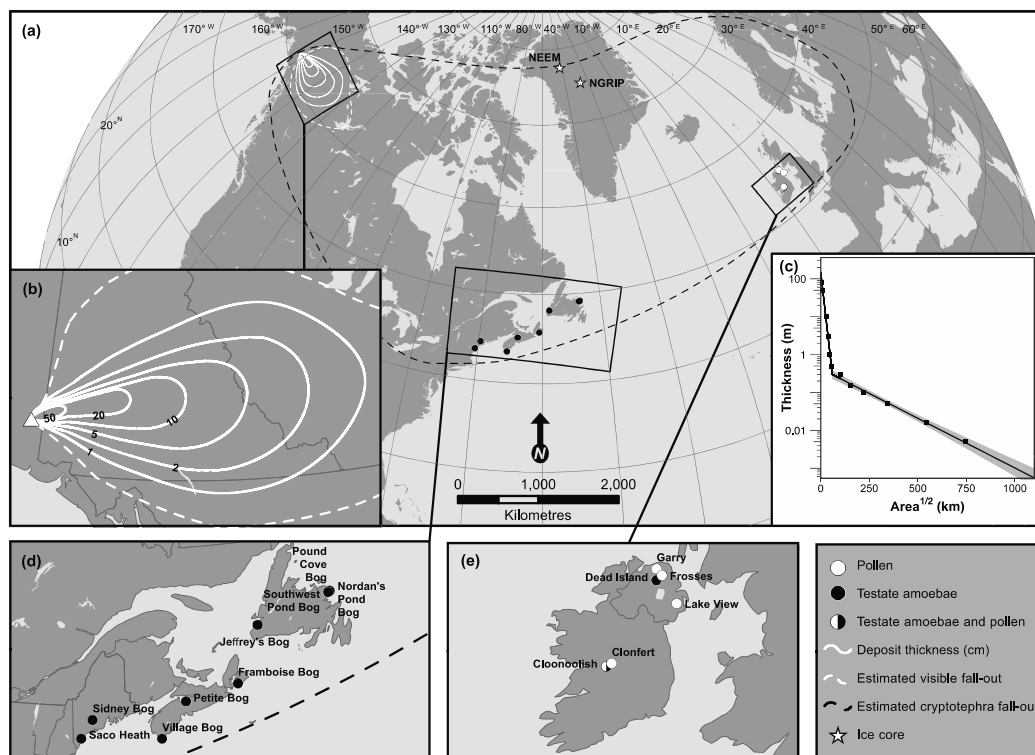


70 **1. Introduction**

71 The 852/3 CE eruption of Mount Churchill in the Wrangell volcanic field, southeast Alaska, was one of the largest
72 first millennium volcanic events, with a roughly estimated eruptive volume of 47 km³ and top plume height of ca.
73 40–45 km (Lerbekmo, 2008). The considerable ash fall-out from this Volcanic Explosivity Index (VEI) 6 Plinian
74 eruption extended eastwards: visible horizons of the ash, termed White River Ash east (WRAe), have been
75 identified >1300 km from the source (e.g. Lerbekmo, 2008; Patterson et al., 2017) and WRAe cryptotephra (non-
76 visible volcanic ash) deposits have been detected in northeastern North America (Pyne O'Donnell et al., 2012;
77 Mackay et al., 2016; Jensen et al., in press; Figure 1a-c). Furthermore, the correlation of the WRAe with the “AD
78 860B” tephra first identified in Ireland (Pilcher et al. 1996) has extended the known spatial distribution of the
79 cryptotephra to Greenland (NGRIP and NEEM ice cores) and western and eastern Europe (e.g., Coulter et al., 2012;
80 Jensen et al., 2014; Watson et al., 2017a, b; Kinder et al., 2020).

81 The ash produced from this eruption caused considerable and long-lasting environmental disturbances in regions
82 proximal to Mount Churchill. For example, the eruption has been linked with changes in vegetation that persisted for
83 ca. 50-150 years in Yukon (Rainville, 2016), multi-centennial changes in peatland ecology in southeast Alaska
84 (Payne and Blackford, 2008) and decreases in aquatic productivity lasting ca. 100 years in southwest Yukon
85 (Bunbury and Gajewski, 2013). These spatial patterns in proximal environmental responses to the 852/3 CE
86 Churchill eruption are diverse. The eruption and its environmental impacts are also suggested to have driven societal
87 changes in the region (Kristensen et al., 2020), notably a decline in indigenous occupancy in the southern Yukon
88 (Hare et al., 2004). In addition, the event may have triggered the southwards migration of people, who brought their
89 culture and Athapaskan language to the US Great Basin and the American Southwest (Mullen, 2012). Several
90 studies have therefore characterized the proximal impacts of this 852/3 CE Churchill eruption, but less is known
91 about the widescale Northern Hemisphere (NH) or global impacts of this large eruption.

92



93

94 **Fig. 1: Site and White River Ash east distribution map with thickness data for volume estimate.**
95 **(a) Location map, highlighting Greenland ice core sites (NEEM = North Eemian, NGRIP = North Greenland Ice Core Project), estimated**
96 **cryptotephra fall-out area, and inset map extents. (b) Isopach map synthesized from distal and proximal isopachs**
97 **(Lerbekmo 1975, 2008). (c) Plot of deposit thickness (on a log scale) against square root area of isopachs ≥ 0.5 cm and two-**
98 **piece exponential fit (black line). The grey shaded area represents the 95% confidence interval of the fitted function. (d)**
99 **Inset map highlighting testate amoebae sites from northeastern North America. (e) Inset map highlighting testate**
100 **amoebae and pollen sites from Ireland.**

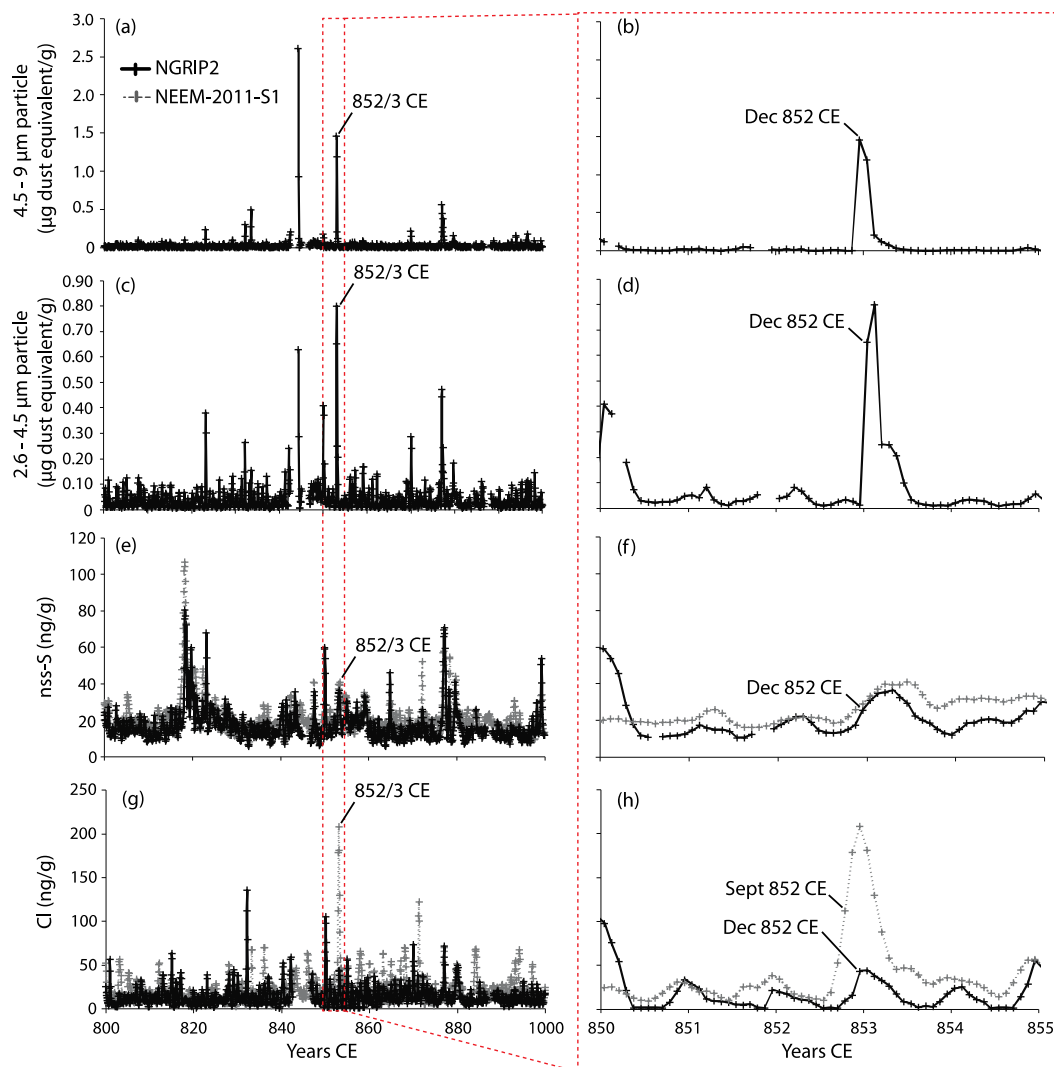
101 Several lines of evidence suggest that the 852/3 CE Churchill eruption occurred in winter, including the stratigraphic
102 context of the tephra in proximal locations (West and Donaldson, 2000), the ash cloud trajectory (Muhs and Budahn,
103 2006) and the timing of ash deposition in Greenland. Cryptotephra from the eruption was identified in the NGRIP
104 and NEEM-2011-S1 ice cores from northern Greenland in ice then dating to 847 CE based on the Greenland Ice
105 Core 2005 (GICC05 chronology; Coulter et al., 2012; Jensen et al., 2014). Based on the revised NS1-2011
106 chronology (Sigl et al. 2015), the event is now dated to the winter of 852/3 CE (Fig 2), and is likely to have occurred
107 between September 852 CE and January 853 CE, with sulfate deposition peaking in early 853 CE (Fig. 2e-f). The
108 eruption also produced large quantities of ash and chlorine, the peak deposits of which are detected a few months
109 prior to the sulfate peak in Greenland (Fig. 2). The NS1-2011 chronology is precise to the calendar year in 939 CE
110 and 775 CE (Sigl et al., 2015) and it is therefore well-constrained over the time period of interest for this Churchill



111 eruption. The resultant conservative age uncertainty associated with the 852/853 CE Churchill eruption is winter
112 852/853 CE \pm 1 calendar year.

113 Large volcanic eruptions have been implicated in global to hemispheric climate change and societal impacts (e.g.
114 Sigl et al., 2015; Stoffel et al., 2015; Büntgen et al., 2016, 2020; Oppenheimer et al., 2018; McConnell et al., 2020)
115 and raise the question of whether the Churchill eruption – amongst the largest magnitude eruptions of the Common
116 Era – also had a far-reaching impact. While extratropical eruptions are often thought to have less impact on climate
117 than tropical eruptions, recent modelling experiments have shown that large extratropical eruptions with injection
118 heights above ~17 km can have a significant hemispheric climate impact (Toohey et al., 2019). The Churchill
119 eruption certainly reached stratospheric heights, but it appears associated with only limited sulfate deposition in
120 Greenland ice cores (Fig. 2e), on the basis of which it is estimated to have produced 2.5 Tg of sulfur (ca. 5 Tg SO₂
121 (Toohey and Sigl, 2017)). This sulfate production estimate of the 852/3 CE Churchill eruption is an order of
122 magnitude less than the Alaskan 43 BC eruption of Okmok (McConnell et al., 2020), which was one of the three
123 largest eruptions, in terms of estimated aerosol forcing, of the last 2500 years (Sigl et al., 2015) and is less than a
124 third of the amount of sulfate produced during the 1991 eruption of Mount Pinatubo (Guo et al., 2004). The 852/3
125 Churchill eruption therefore provides a test case for investigating whether the event had the potential to impact
126 climate and society on the basis of the moderate estimated volcanic emissions, and the degree to which paleoclimate
127 reconstructions and historical records demonstrate environmental changes that might be regarded as consequences of
128 the eruption.

129 Given the extent of the Churchill WRAe isochron in glacial and terrestrial environments spanning North America
130 and western Eurasia, our study serves dual purposes. Our first aim is to examine potential NH impacts of the 852/3
131 CE Churchill eruption on climate, terrestrial environments and societies, using modelled forcing data, climate
132 simulations, palaeoenvironmental reconstructions and historical records. Our second aim is to use the WRAe tephra
133 isochron as a pinning-point between inter-continental palaeoenvironmental records to characterize and compare
134 regional expressions of climate change near the outset of the Medieval Climate Anomaly (MCA), a period of
135 increased temperatures ca. 950–1250 CE (Mann et al., 2008; 2009). The WRAe isochron from the 852/3 CE
136 Churchill eruption is therefore aptly placed to identify leads and lags in MCA climate responses and improve
137 characterizations of the spatial and temporal extent of this warm period. We similarly use the tephra isochron to
138 critique the timing of land-use practices, inferred from pollen records, during a period of known societal
139 reorganisation, to determine the extent to which climate change played a role in socio-economic transformation.



140

141 **Fig. 2:** Geochemical characteristics of the 852/3 CE Churchill eruption based on concentrations of (a-b) ash inferred from
142 4.5–9 μm particles, (c-d) ash inferred from 2.6–4.5 μm particles, (e-f) non-sea salt sulfate (nss-S), and (g-h) chlorine (Cl),
143 from Greenland ice cores NGRIP2 and NEEM-2011 S1 (Jensen et al., 2014) on the NS1-2011 chronology (Sigl et al., 2015).



144 2. Methods

145 2.1 Revised eruption volume estimate and magnitude

146 Despite the considerable magnitude of the eruption that deposited WRAe, there has not been a spatially consistent
147 estimate of its volume or magnitude using established methods (e.g., two-piece exponential function, Pyle 1989;
148 Weibull function, Bonadonna and Costa, 2012). The most recent volume estimate for WRAe (Lerbekmo, 2008) used
149 disparate isopach maps for the proximal and distal regions of the deposit and the uncertainty assessment was limited.
150 Here we construct an updated isopach map for WRAe using a GIS-based synthesis of Lerbekmo's distal and
151 proximal isopachs ≥ 0.5 cm (Lerbekmo, 1975, 2008; Fig. 1a-b). We then calculate an updated tephra volume
152 estimate by assuming deposit thinning follows a two-piece exponential function (Pyle, 1989; Fierstein and
153 Nathenson, 1992). Dense rock equivalent (DRE) is calculated assuming a representative deposit density of 1.19 kg
154 m^{-3} and a dense rock density of 2.5 kg m^{-3} (following Lerbekmo, 2008). These estimates of WRAe volume are the
155 first to assess function-fitting confidence, allowing the mathematical model to account for the uncertainty of the
156 deposit volume, especially < 0.5 cm.

157 2.2 Reconstructed forcing potential: stratospheric aerosol optical depth and radiative forcing

158 We develop a primary forcing reconstruction for the 852/3 CE Churchill eruption using the EVA(eVolv2k) 550 nm
159 stratospheric aerosol optical depth (SAOD) reconstruction (Toohey and Sigl, 2017). Detailed explanations of the
160 model selection and set-up are provided in Appendix A. We also generate a second SAOD reconstruction using the
161 EVA_H model, which is an extension of the Easy Volcanic Aerosol Model (EVA, Toohey et al., 2016), that
162 accounts for the SO_2 injection latitude and altitude and is calibrated using a more extensive observational dataset
163 than EVA (Aubry et al., 2020). The EVA_H reconstruction uses the same SO_2 mass as EVA, the latitude of
164 Churchill (61.38°N), and an injection altitude of 31.5 km. The injection altitude is based on the isopleth-derived top
165 height estimate of 40–45 km from Lerbekmo (2008) corrected by a factor of 0.725 to be representative of the altitude
166 of the spreading umbrella cloud instead of the cloud top (Carey and Sparks, 1986). We also provide a 95%
167 confidence interval on EVA_H prediction that accounts for uncertainties in model parameter (Aubry et al., 2020),
168 the SO_2 mass uncertainty ($5 \pm 2.5 \text{ Tg SO}_2$, Toohey and Sigl, 2017), and an assumed uncertainty of 30% on the
169 injection height.

170 2.3 Climate model simulation

171 Climate conditions were simulated using the Community Earth System Model version 1.2.2 (CESM; Hurrell et al.,
172 2013). The ensemble simulation consists of 20 ensemble members performed to study the impacts of the 852/853
173 CE Churchill eruption on climate. To generate the ensemble members, initially a seamless transient simulation is run
174 from 1501 BCE (Kim et al., 2021) with time-varying orbital parameters (Berger, 1978), total solar irradiance (Vieira
175 et al., 2011; Usoskin et al., 2014, 2016), greenhouse gases (Joos and Spahni, 2008; Bereiter et al., 2015), and
176 volcanic forcing from the HolVol v.1.0 (Sigl et al., 2021) and eVolv2k (Toohey and Sigl, 2017) databases. The



177 necessary prescribed spatio-temporal distribution of volcanic sulfate aerosol for the simulation is generated using the
178 EVA Model (Toohey et al., 2016) and follows the same procedure employed by McConnell et al. (2020) and Kim et
179 al. (2021). The simulations used for the analysis have the spatial resolutions of approximately $1.9^\circ \times 2.5^\circ$ for the
180 atmosphere and land, and $1^\circ \times 1^\circ$ for the ocean and sea ice. The vertical grids use 30 levels for the atmosphere, 60
181 levels for the ocean and 15 levels for the land. The output data are provided at a monthly resolution. More details of
182 the simulations investigating the impact of the 852/3 CE Churchill eruption on climate are provided in Appendix B.

183 The anomalies of temperature and precipitation are calculated by subtracting the 845–859 CE multi-year monthly
184 means from the values at each grid point for the initial condition ensemble simulation. From these anomalies, the
185 seasonal means of each individual ensemble simulation are computed as well the ensemble means of 20 member
186 simulations. NH summer conditions reported here refer to climate conditions of June-July-August (JJA), and winter
187 conditions refer to December (of the previous year)-January February (of the reported calendar year) (DJF).

188 To test the statistical significance of changes in temperature and precipitation after the 852/3 CE Churchill eruption,
189 we use the Mann-Whitney U-test (for an example, refer to Kim et al., 2021) that compares the distributions of two
190 variables between the pre-eruption period (845–852 CE) and each individual after-eruption year (853, 854, and 855
191 CE). More details of the procedure for the significance tests are provided in Appendix B. In addition, the variability
192 of the spatially-averaged ensemble means of temperature and precipitation is compared with the pre-eruption
193 ensemble by assessing whether the variability falls within the range of two standard deviations from the means of
194 the pre-eruption period.

195 **2.4 Northern hemisphere (NH) tree-ring summer temperature and drought reconstructions**

196 NH summer (JJA) temperatures in the 850s CE were reconstructed using 13 NH tree-ring width and 12 maximum
197 latewood density chronologies (Guillet et al., 2017, 2020). Full details of the nested principal component regression
198 (PCR) used to reconstruct NH JJA temperature anomalies (with respect to 1961–1990) and the model calibration are
199 provided in Appendix C. To place the summer temperature anomalies within the context of climate variability at the
200 time of major volcanic eruptions, we filtered the final reconstruction by calculating the difference between the raw
201 time series and the 31-year running mean. Further investigation of volcanic-forced cooling was facilitated by
202 filtering the original reconstructions using a 3-year running mean to filter out high-frequency noise. To estimate the
203 spatial variability of summer cooling induced by the winter 852/3 CE eruption, we also developed a 500–2000 CE
204 gridded reconstruction of extratropical NH summer temperatures (more details are provided in Appendix C).

205 Estimated soil moisture anomalies for the 9th century are extracted from tree-ring reconstructions of the gridded
206 summer (JJA) Palmer Drought Severity Index (PDSI) over North America, Europe, and the Mediterranean (Cook et
207 al. 2010, Cook et al. 2015). The PDSI metric integrates the influence of both precipitation, evapotranspiration, and
208 storage on soil moisture balance throughout the year and is normalized so that values can be compared across regions
209 with a range of hydroclimate conditions. Positive values indicate anomalously wet conditions, while negative values



210 are anomalously dry for that location, and normal conditions are set to zero. Tree-ring PDSI reconstructions in North
211 American and Euro-Mediterranean Drought Atlases are developed using the point-by-point regression approach
212 described by Cook et al. (1999).

213 **2.5 Testate amoebae peatland water table depth (i.e. summer effective precipitation) reconstructions**

214 Testate amoebae are a well-established palaeoenvironmental proxy used to reconstruct past hydroclimatic variability
215 in ombrotrophic (rain-fed) peatlands because species assemblages predominantly respond to changes in peatland
216 surface moisture during summer months, and tests are preserved in the anoxic peat strata (e.g. Woodland et al.,
217 1998; Mitchell et al., 2008). For this study, testate amoeba analysis was completed on cores obtained from 11
218 ombrotrophic peatlands located in Maine (n = 2), Nova Scotia (n = 3), Newfoundland (n = 4) and Ireland (n = 2)
219 (Fig. d-e), in which the presence of the WRAe has been confirmed by electron probe microanalysis of the volcanic
220 glass (Swindles et al., 2010; Pyne O'Donnell, 2012; Mackay et al., 2016; Monteath et al., 2019; Jensen et al., in
221 press; Plunkett., unpublished; Appendix D). The peatland sampling approaches used here are outlined in Mackay et
222 al. (2021), and testate amoeba analysis was completed using standard protocols (Hendon and Charman, 1997; Booth
223 et al., 2010) across all cores at multidecadal resolution (approximately 40-years), equating to 2 to 4 cm intervals.
224 Testate amoebae were extracted from 1 cm³ subsamples following standard procedures (Hendon and Charman,
225 1997; Booth et al., 2010). At least 100 individual tests were identified (Payne and Mitchell, 2009) per sample using
226 the taxonomy of Charman et al. (2000) and Booth (2008). Testate amoebae water table depth (WTD) reconstructions
227 were obtained using the tolerance-downweighted weighted averaging model with inverse deshrinking (WA-Tol inv)
228 from the North American transfer function of Amesbury et al. (2018). Reconstructed WTD values were normalised
229 for comparative purposes (Swindles et al., 2015; Amesbury et al., 2016). Two WTD reconstructions exist from
230 different coring locations on Sidney Bog, Maine (Clifford and Booth, 2013; Mackay et al., 2021); therefore, a
231 composite record was constructed based on interpolated average WTD values (Appendix E). Two WTD
232 reconstructions also exist from different coring locations on Saco Heath (Clifford and Booth, 2013; Mackay et al.,
233 2021), however, a composite record was not created for this site since one record contains a pronounced hiatus
234 below the WRAe horizon, relating to a burning event (Clifford and Booth, 2013). The Saco record presented within
235 this study contains no evidence of a hiatus until later in the record, ca. 1000 CE, when the accumulation rate
236 decreases (Appendix D). Core chronologies were developed using Bayesian analysis within the R package
237 “BACON” (Blaauw and Christen, 2011) based on ¹⁴C dates and tephrochronologies (Appendix D). Radiocarbon
238 dates were calibrated using the NH IntCal20 calibration curve (Reimer et al., 2020) and are reported as Common Era
239 dates.

240 **2.6 Pollen vegetation reconstructions**

241 The 9th century in Ireland was a time of significant socio-economic reorganisation and possibly population decline
242 (Kerr et al., 2009; McLaughlin et al., 2018; McLaughlin, 2020). To investigate the extent to which these events may
243 have been driven the effects of either the 852/3 CE eruption or the transition to the MCA, we compiled land-use



244 proxy data from five pollen records (Fig. 2e) that included the Churchill (“AD860B”) tephra as a chronological tie-
245 point (Hall, 2005; Coyle McClung, 2012; Plunkett, unpublished data). Raw data were recategorized by biotope, with
246 a specific focus on the ratio of arboreal pollen (AP) to non-arboreal pollen (NAP), and the representation
247 (percentage of total dryland pollen) of taxa associated with pastoral or arable farming. Age-models were constructed
248 for each site based on tephrochronological and ¹⁴C dates in the same manner used for the testate amoebae records
249 (Sect. 2.5).

250 **2.7 Historical records**

251 A wide range of written sources were examined to collate the extant historical record of climate and weather for the
252 period 850–856 CE. This survey focused on Europe – northwestern insular Europe (Irish and Anglo-Saxon annals)
253 and continental Europe (annals and histories covering Byzantine, Carolingian and Umayyad lands) – southwest
254 Asia, North Africa (Abbasid and Byzantine texts), and Tang-era eastern China. To place the 852/3 CE eruption in a
255 wider context where effects of the eruption are apparent, we employ evidence for large subsistence crises
256 (‘famines’) and seemingly more circumscribed crises (‘lesser food shortages’) spanning 800–900 CE reported in
257 Carolingian sources, which comprise one of the densest records of subsistence crises extant for the 9th century
258 anywhere (Newfield 2013, Devroey 2019).

259 **3. Results**

260 **3.1 Volume estimate and magnitude**

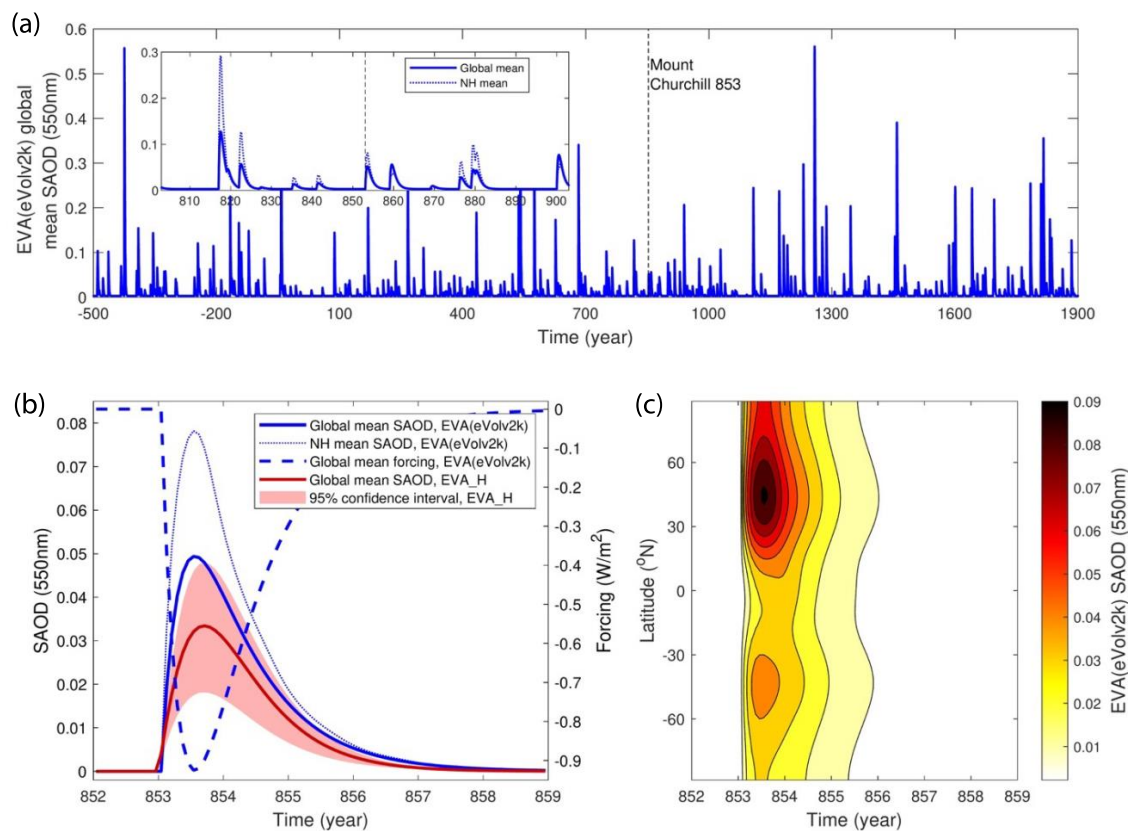
261 WRAe deposit bulk tephra volume was modelled as a mean value of 49.3 km³, with an estimated 95% confidence
262 interval (CI) of 39.4–61.9 km³. The deposit constituted a mean dense rock equivalent (DRE) volume of 23.6 km³
263 (95% CI, 18.8–29.6 km³ at 95% confidence) and weighed about 48.7 Gt (95% CI, 38.9–61.2 Gt at 95% confidence).
264 Such volumes and masses indicate the eruption that deposited WRAe was of volcanic explosivity index (VEI) 6 and
265 a magnitude (M) of around 6.7 (95% CI, 6.6–6.8 at 95% confidence).

266 **3.2 Climatic forcing potential of 852/3 CE Churchill eruption**

267 The EVA(eVolv2k) reconstructed stratospheric aerosol optical depth (SAOD) for the 852/3 CE eruption is relatively
268 moderate, with a peak aerosol optical depth perturbation of 0.049 in terms of global mean, and 0.078 in terms of
269 North Hemisphere (NH) mean (Fig. 3a-b). In comparison, the global mean SAOD following the Pinatubo 1991
270 eruption was 2–3 times larger (Thomason et al., 2018) and the reconstructed global mean SAOD for the largest
271 eruptions of the Common Era (Fig. 3a) reaches 0.3–0.6 (e.g., 0.56 for the Samalas 1257 CE eruption). For the 9th
272 century alone, four volcanic events have a peak global mean SAOD exceeding that of the 852/3CE Churchill
273 eruption. The EVA_H reconstruction (Fig. 3b), which accounts for the SO₂ injection latitude and altitude, suggests
274 an even smaller global mean SAOD perturbation of 0.033 (95% confidence interval 0.018–0.048). In terms of the
275 latitudinal distribution of the SAOD perturbation, both the EVA (Fig. 3c) and EVA_H (not shown) reconstructions



276 produce a SAOD perturbation that is much stronger in the NH but propagates to the tropics and Southern
277 Hemisphere. Based on the EVA(eVolv2k) SAOD estimate and using volcanic forcing efficiency from Marshall et al.
278 (2019), the global mean radiative forcing peaked at -0.92 W m^{-2} (Fig. 2b), a value roughly one-third that for the
279 Mount Pinatubo 1991 eruption (e.g., Schmidt et al., 2018).



280

281 **Fig. 3: Stratospheric aerosol optical depth (SAOD, 550 nm) reconstructed for the Churchill 852/3 eruption. (a) The 500**
282 **BCE–1900 CE EVA(eVolv2k) reconstructed global mean SAOD, with the inset showing details for the 803–903 period**
283 **and both the global mean and North Hemisphere (NH) mean SAOD. (b) The same time series for the 852–859 CE period,**
284 **during which the Churchill 852/3 eruption is clearly seen. This panel also shows the global mean radiative forcing**
285 **reconstructed from the EVA(eVolv2k) SAOD, and an alternative SAOD reconstruction using the EVA_H model, an**
286 **extension of EVA that accounts for the SO_2 injection and latitude for reconstructing global mean SAOD. (c) Time-latitude**
287 **evolution of SAOD as reconstructed with EVA(eVolv2k).**

288 3.3 Annually resolved climate reconstructions

289 3.3.1 NH tree-ring-based climate reconstructions

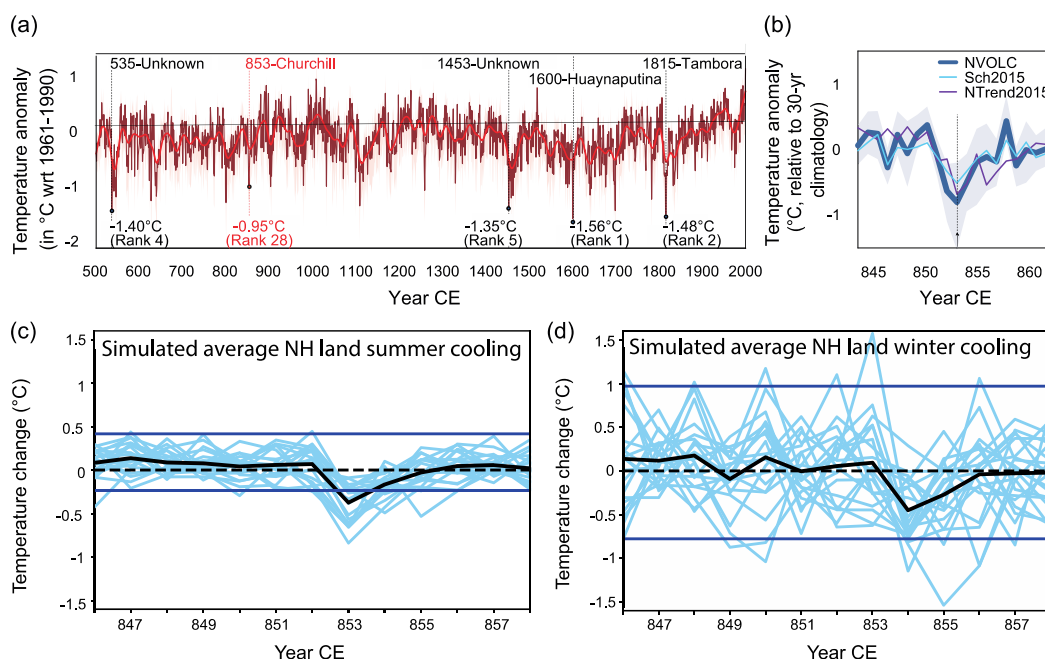
290 NH summer temperature reconstructions based on tree-ring records reveal long-term decadal-scale temperature
291 fluctuations between 500–2000 CE (Fig. 4a). All tree-ring based NH JJA reconstructions contain a short-lived
292 decreasing temperature trend from 851 CE that peaks in 853 CE, with temperatures anomalies (relative to 1961–



293 1990) reaching -0.85°C in the filtered reconstruction (Fig. 4b). The 1961–1990 reference period used for the tree-
294 ring reconstructions was 0.1°C warmer than the modelled climate simulation reference period (845–852 CE). Cold
295 temperatures persist in 854 CE (with -0.65 and -0.5°C in the filtered and unfiltered reconstructions, respectively),
296 before attaining pre-eruption levels in 855 CE (Fig. 4b). The cold temperature anomaly observed in 853 CE is
297 significant and among the 5th percentile of coldest values in the filtered and unfiltered reconstructions and very close
298 to the 1st percentile of the coldest values in the distribution of the filtered reconstruction (Appendix F). Over the
299 period 500–2000 CE, 853 CE ranks as the 28th and 18th coldest events in the unfiltered and filtered reconstructions,
300 respectively (Fig. 4a). Further investigation of volcanically forced cooling as examined using a 3-year running mean
301 places 853–856 CE as the 11th coldest 3-year period between 500 and 2000 CE (Appendix G). An examination of the
302 30 coldest 3-year periods from the filtered time series highlights that all such periods are preceded by an eruption or
303 a group of eruptions, and 19 of these eruptions occur within two years before the ranked cold periods (Appendix G).

304 Spatial patterns of the hemisphere-wide JJA cooling in the early 850s are complex (Fig. 5a): generally cold
305 conditions prevailed over western and central Europe as well as Scandinavia (anomalies exceeding -0.8°C with
306 respect to the 1961–1990 mean) – and to a lesser extent Alaska (with peak cooling in 854 CE) – between 851 and
307 854 CE. The peak cooling in the NH in 853 and 854 CE seen in Fig. 4b is explained by the strong cooling of Central
308 Asia and vast parts of Siberia in the same years (Fig. 5a). While clear warming is evident in central and western
309 Europe and Scandinavia in 855 CE, low temperatures persist in Central Asia in 855 CE.

310 Summer PDSI reconstructions based on tree-ring records reveal a shift from wet to drier conditions in parts of
311 western Europe in 854 CE which persists into 855 CE (Fig. 5d). Wetter conditions in 853 CE in northern Europe and
312 dry anomalies in North Africa and parts of the Mediterranean are potentially indicative of a positive phase of the
313 North Atlantic Oscillation. By 855 CE, dry conditions in northern and western Europe and, in 855 CE in the eastern
314 United States are more similar to the pattern expected during a negative phase of the North Atlantic Oscillation
315 (Anchukaitis et al. 2019). Eastern North American tree-ring moisture reconstructions however are also consistently
316 dry from 852 through 855 CE. Tree-ring records in the western half of the continent reveal a mixed PDSI anomaly,
317 generally indicating wetter conditions to the southwest and drier in the northwest, reminiscent of the moisture
318 anomalies during a El Niño event in the tropical Pacific (Fig. 5d).



319

320 **Fig. 4 (a-b)** Tree-ring-derived temperature reconstructions around the time of the 852/3 CE Churchill eruption: (a)
321 Unfiltered NH extra-tropical land (40–90°N) summer temperature anomalies (with respect to the period 1961–1990) since
322 500 CE. The red lines represent the interannual temperature anomaly variations and the grey lines represent the 95%
323 bootstrap limits. (b) Comparison of the NVOLC cooling observed after the winter 852/3 CE eruption in the
324 reconstruction filtered with a 31-yr running mean with other NH reconstructions, Sch2015 (Schneider et al., 2015) and N-
325 TREND2015 (Wilson et al., 2016). Grey shaded area represents the uncertainty associated with NVOLC temperature
326 anomaly reconstruction. (c-d) Simulated NH climate before and after the 852/3 Churchill eruption: (c) 846–858 CE time
327 series of spatially-averaged NH extratropical (15–90°N latitudes) land temperature anomalies from 20 ensemble
328 simulations for summer (JJA), and (d) winter (DJF) in light blue lines. The thick black lines indicate the ensemble means,
329 and the horizontal blue lines represent two standard deviations from the ensemble means of the 845–852 CE pre-eruption
330 period. For comparative purposes, the 1961–1990 reference period used for the tree-ring reconstructions (a-b) was 0.1°C
331 warmer than the modelled climate simulation reference period (c-d) of 845–852 CE.

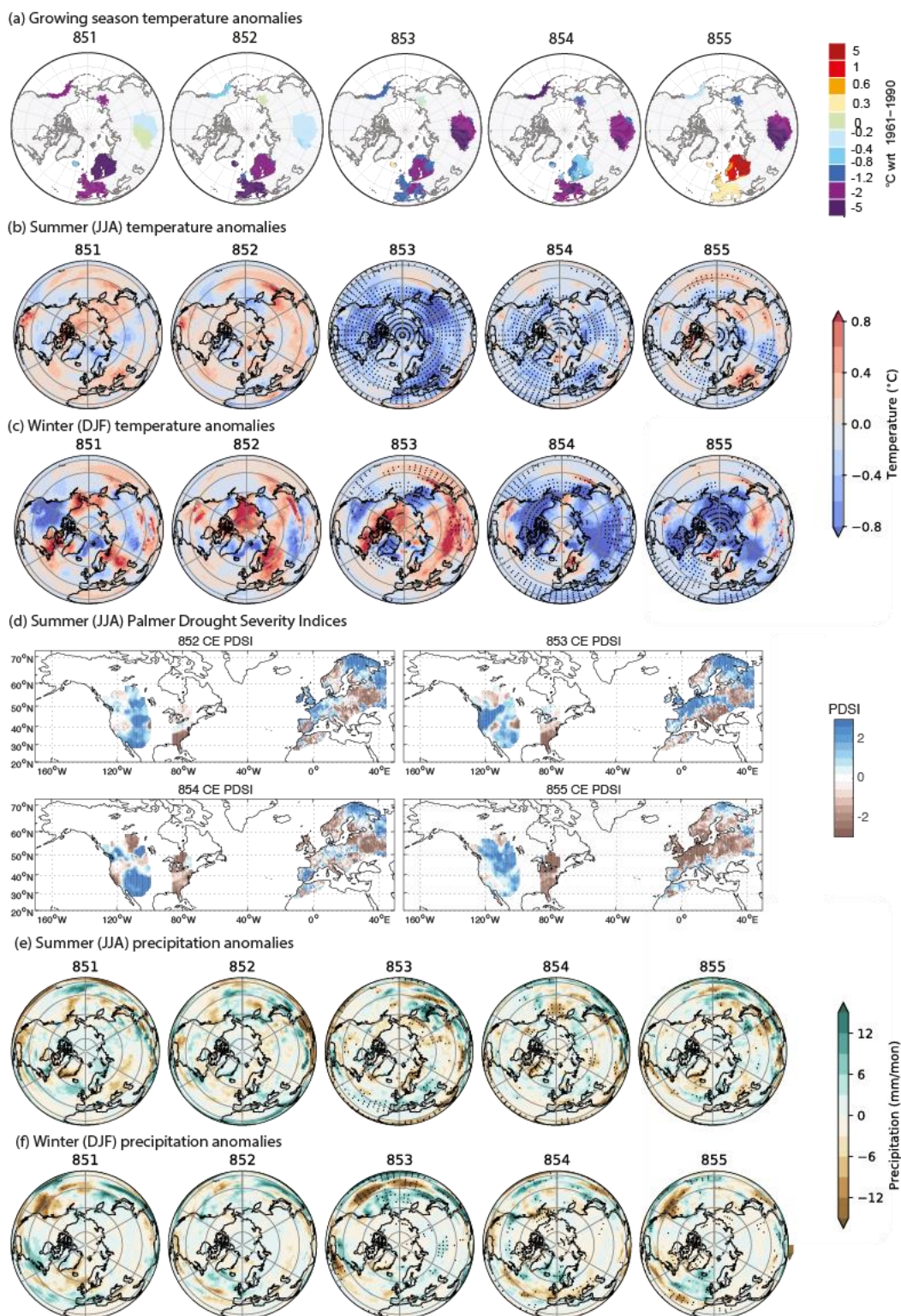
332 3.3.2 NH modelled climate scenarios

333 Simulated summer (JJA) temperature anomalies derived from the CESM reveal a widespread cooling in the NH
334 extratropical regions in 853 CE that reaches an ensemble mean value of approximately $-0.29\text{ }^{\circ}\text{C}$ (Fig. 4c). In many
335 extratropical regions, the decrease in summer temperature is statistically different to the pre-eruption period at a 5%
336 confidence level (Fig. 5b) and the ensemble means of the temperature anomalies in summer 853 CE are greater than
337 two standard deviations from the 845–852 CE pre-eruption period mean, placing it among the 2nd percentile of the
338 coldest simulated temperatures. Cool conditions mainly persist into 854 CE, albeit with smaller temperature anomalies
339 (NH land average cooling of $-0.15\text{ }^{\circ}\text{C}$; Fig. 4c), but by 855 CE, warm temperature anomalies return, for example, to
340 parts of southeast Europe, northeast Canada and the North Pacific. Modelled winter (DJF) temperature anomalies
341 reveal a cooling trend that starts and peaks approximately $-0.32\text{ }^{\circ}\text{C}$ in 854 CE and recovers by 856 CE (Fig. 4d).
342 Modelled winter (DJF) temperature anomalies reveal a hemispheric mean, ensemble mean cooling anomaly that peaks



343 at approximately -0.32°C in 854 CE and recovers by 856 CE (Fig. 4d). The ensemble mean winter cooling in 854 CE
344 is more spatially variable than the 853 CE summer cooling, with warm temperatures anomalies persisting in parts of
345 Scandinavia, central Europe and western North America during the winter months (Fig. 5c). The variability among
346 the ensemble members during the after-eruption period (853–855 CE) is high, with the NH land surface temperature
347 means ranging from -0.84 to 0.25°C in summer and -1.54 to 1.57°C in winter.

348 The modelled summer (JJA) and winter (DJF) precipitation anomalies vary spatially and temporally between 851–
349 855 CE (Fig. 5e-f), although the post-eruption variability of precipitation is statistically indistinguishable from that
350 of the pre-eruption period. Parts of western Europe show slightly drier conditions in winter 853 CE, with wetter
351 conditions prevalent in western Scandinavia. The summer of 853 CE is characterised by slightly wetter conditions in
352 parts of western Europe (Fig. 5e). The spatially-averaged ensemble mean of precipitation indicates that all variation
353 occurs within one standard deviation of the pre-eruption period means (Appendix H); there is therefore no obvious
354 statistical differences between modelled summer and winter precipitation patterns associated with the 852/853 CE
355 Churchill eruption in the NH.





357 **Figure 5: Reconstructed and simulated NH spatial patterns of temperature and precipitation anomalies (a) Growing**
358 **season gridded (1° lat \times long) temperature anomalies reconstructed over the NH ($40\text{--}90^\circ$ N) between 851 and 855 CE**
359 **based on tree-ring reconstructions. Scale extends from red, representing a temperature increase, to purple, representing a**
360 **temperature decrease. (b) Annually-averaged ensemble means of simulated temperature anomalies for summer, and (c)**
361 **winter. (d) Spatial patterns of boreal summer (June–August) Palmer Drought Severity Index (PDSI) anomalies (Cook et**
362 **al. 2010, Cook et al. 2015). The PDSI scale extends from blue, representing wetter-than-normal conditions at that**
363 **location, to brown, representing drier-than-normal conditions. (e) Annually-averaged ensemble means of simulated**
364 **precipitation anomalies for summer, and (f) winter. Dotted regions in (b), (c), (e) and (f) indicate where the changes are**
365 **statistically significant (based on the Mann-Whitney-U-test) compared to the pre-eruption period.**

366 **3.4 Multidecadal scale palaeoenvironmental reconstructions**

367 **3.4.1 Peatland hydrological change associated with WRAe deposition**

368 The compilation of WTD data in peatlands indicates no consistent response at the time of the WRAe deposition
369 (Fig. 6). Both Irish peatlands record wet conditions relative to the preceding decades at the time of WRAe
370 deposition, but the Dead Island record indicates a subsequent long-term drying whilst Cloonoolish records a
371 temporary drying before a shift to wetter conditions. Two of the three peatlands in eastern Newfoundland record
372 wetter conditions following the WRAe deposition. Jeffrey's Bog in southwestern Newfoundland and the peatlands
373 in Nova Scotia become drier following the eruption but the duration and magnitude of the water table lowering vary
374 between peatlands. For example, the longer-term drying trends in Jeffrey's Bog, Framboise Bog and Villagedale
375 Bog persist over approximately 200 years whilst the drying in Petite Bog is less pronounced and shorter-lived (ca.
376 50 years). The peatlands in Maine register a temporary shift to wet conditions following the WRAe deposition.

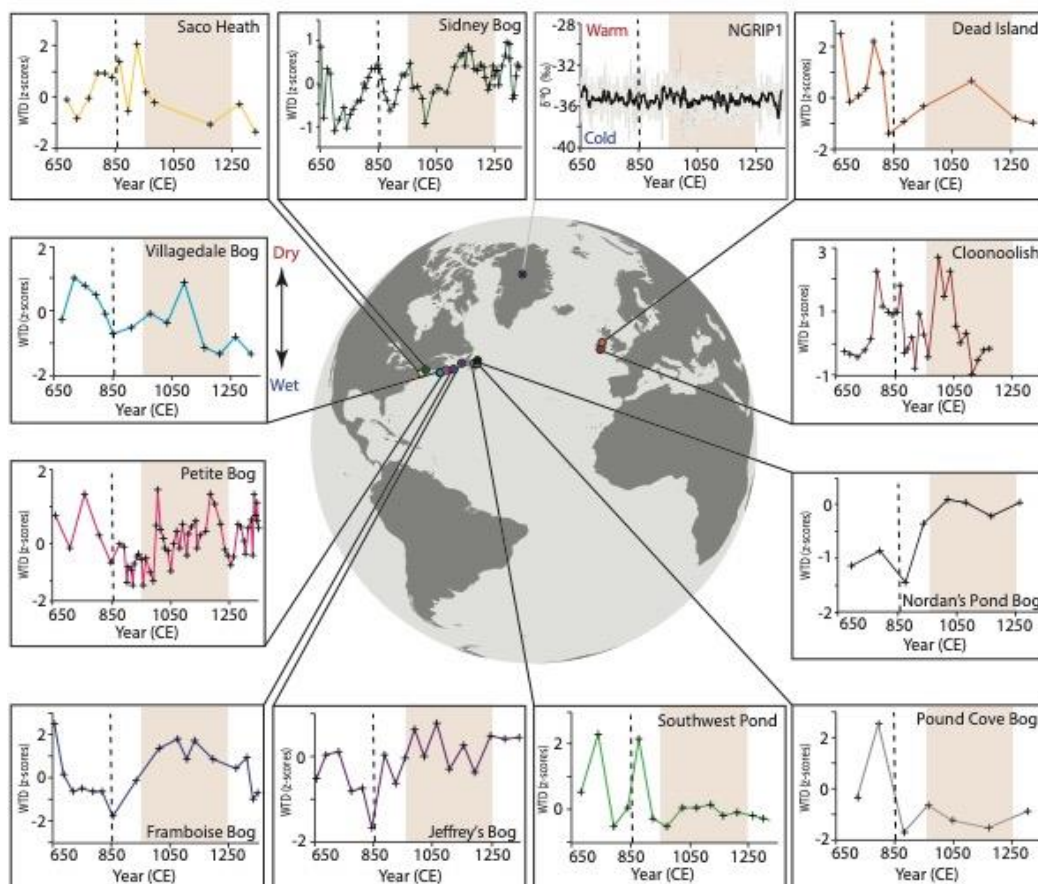
377 Although most of the sites reflect centennial-scale trends in WTD, the higher temporal resolution of Petite and
378 Cloonoolish bogs (11 and 12.5 years respectively) allow decadal-scale responses of the peatlands following the
379 eruption to be considered. Each bog experienced a short-term change towards drier conditions before returning to
380 the prior trend to wetter conditions, but the scale of each hydrological shift lies within the levels of variability of the
381 WTD records.

382 **3.4.2 Peatland hydrological change during the Medieval Climate Anomaly**

383 We find no consistent MCA signal registered in the peatland WTD reconstructions (Fig. 6). Our peatland WTD
384 records indicate that the medieval period was characterised by variable hydrological conditions. The onset of
385 changes towards drier conditions, which may signal the warm Medieval Climate Anomaly, varies temporally and
386 spatially. The earliest dry shift starts ca. 900 CE in northern Nova Scotia (Framboise Bog) and some records from
387 Newfoundland (Jeffrey's Bog and Nordan's Pond Bog), whilst this hydroclimatic change is registered ca. 100 years
388 later in records from southern and central Nova Scotia (Villagedale Bog, Petite Bog), Maine (Sidney Bog) and
389 Ireland (Cloonoolish). All records in this study register temporary wet shifts at approximately 850 CE and 1050-
390 1150 CE, although the extent and durations of the wet shifts vary. The presence of the WRAe isochron conclusively
391 demonstrates that the onset of the wet shift ca. 850 CE is not synchronous. There is also a high degree of spatial
392 variability between records from sites proximal to one another, with some recording contradictory hydrological



393 conditions, such as Saco Heath and Sidney Bog in Maine and Nordan's Pond Bog, Pound Cove Bog and Southwest
394 Pond Bog in Newfoundland.



395

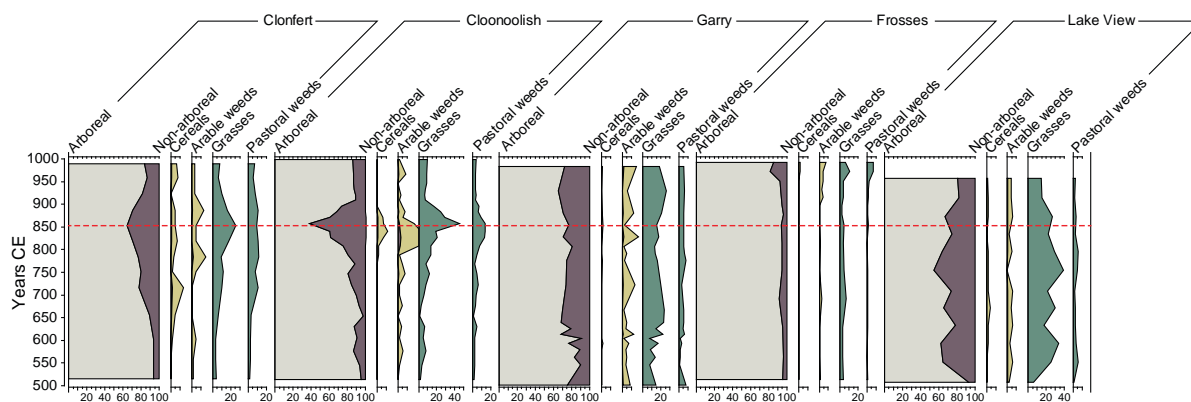
396 **Fig. 6:** Available moisture reconstructions from terrestrial and glacial archives containing the WRAE from the North
397 Atlantic region. Records have been developed using $\delta^{18}\text{O}$ isotopes from NGRIP1 (Vinther et al., 2006), where the black
398 line represents decadal-scale moving average and data are plotted on NS1-2011 chronology (Sigl et al., 2015; for detailed
399 9th century NGRIP1 $\delta^{18}\text{O}$ isotopes see Appendix J), and peatland water table depths inferred from testate amoebae.
400 Dashed vertical line represents the WRAE and the pink shaded box represents the MCA time period based on the Mann
401 et al. (2009) timings (950–1250 CE). Sites have been arranged clockwise with Irish records (Dead Island and Cloonoolish)
402 located on the top right of the diagram followed by North American sites from north-east to south-west with records from
403 Newfoundland (Nordan's Pond Bog, Pound Cove Bog, Southwest Pond and Jeffrey's Pond), Nova Scotia (Framboise Bog,
404 Petite Bog, Villagedale Bog) and Maine (Saco Heath and Sidney Bog) and finally the Greenland NGRIP1 record (top of
405 the diagram).
406



407 3.4.3 Vegetation reconstructions

408 Pollen records from Ireland show considerable variability in the intensity and extent of farming (Fig. 7). The WRAe
409 deposition from the 852/3 CE eruption coincides with the pinnacle of land clearance (reduced arboreal pollen) in
410 central Ireland (Clonfert and Cloonoolish bogs), after which pastoral and arable indicators start to decline as
411 woodland expands. Sites in the northeast of Ireland show less coherent trends than those in central Ireland. At Garry
412 Bog, arable weeds temporarily dip at the time of the eruption, although cereals are still evident. In contrast, evidence
413 for farming is very limited at nearby Frosses Bog, highlighting the localised nature of land use in the vicinity of
414 Garry. At Lake View, moderate levels of farming are recorded, and these increase slightly following the eruption
415 before a decline in activity begins later in the century. The spatial diversity in the pollen records (even within a
416 single region) demonstrates that changes in land-use in the 9th century cannot be attributed to any one environmental
417 trigger, and very likely reflect differences in local-to-regional economic organisation and demographic pressures.

418



419 **Fig. 7: Summary pollen records from five sites in Ireland, showing the ratio of arboreal to non-arboreal (dryland) taxa**
420 **and indicators of arable and pastoral environments. Cereal and arable weed curves are shown with a ×10 exaggeration.**
421 **The red dashed line indicates WRAe.**

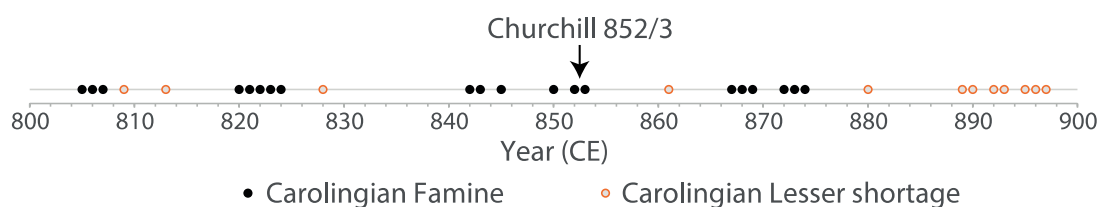
422 3.5 Historical records

423 Historical records from Europe characterize the 850s CE as time of climate instability (Table 1). Carolingian sources
424 observe severe winter flooding in western Germany in 849-850 CE, and severe summer heat, drought and a *fames*
425 (food shortage) in 852 CE (Newfield, 2010; Haldon et al., 2018). Immediately following the 852/3 CE eruption,
426 there is contemporary evidence for a severe famine – such that horse flesh was eaten – which the Annals of Xanten
427 specify took place in Saxony in 853 CE, though beginning possibly in 852 CE (Newfield, 2010; Haldon et al.,
428 2018). The eyewitness annalist of the Annals of Fulda noted that in 855 CE, ‘unusually changeable weather brought
429 loss to many through whirlwinds, storms and hailstorms’. The Annals of St Bertin describe the winter of 856 CE as
430 severe and dry, being also accompanied by a severe epidemic, ‘which consumed a great part of humanity’
431 (Newfield, 2010). Heavy snowfall is reported in Ireland for 23 April 855 CE, with extreme cold implied by frost and



432 load-bearing ice across the winter of 855/6 CE and 856 CE was also deemed a tempestuous and harsh year in
433 Ireland. A severe windstorm occurred in 857 CE and autumn weather in 858 CE characterised as wet and destructive
434 to agriculture in Ireland. A potentially less reliable source (the Fragmentary Annals of Ireland) also reported a
435 famine in the autumn of 858 CE (Ludlow, 2010; Ludlow et al., 2013). The Xanten annalist recorded a great
436 epidemic in 857 CE in northwest Germany, causing ‘swelling bladders’ (or ‘swelling tumours’) and ‘festering sores’
437 that putrefied limbs (Newfield, 2010). While disputable, this epidemic has long been identified as one of ergotism
438 (Hirsch, 1885; Duby, 1974), which is caused by ingestion of the ergot fungus of rye and other grains and is more
439 common in cold and wet growing seasons (Kodisch et al., 2020). The St Bertin annalist reported the epidemic in 858
440 CE. That year too, in May, such a heavy rain fell that the river Meuse burst its banks, flooding Liege (present-day
441 Belgium) and tearing down buildings (Table 1).

442 A wider chronological consideration of the Carolingian evidence reveals that food shortages occurred in several
443 other decades of the 9th century in Carolingian Europe (Fig. 8). This observation reinforces the point that a
444 correspondence (or near-correspondence) between the dating of the Churchill eruption and the documented events of
445 the 850s CE certainly does not confirm a causal linkage. Some food crises of the 9th century were, moreover, vast
446 and longer lasting than those (reliably) documented here for the 850s, with the Carolingian sources also observing
447 widespread crises associated with climate anomalies in the 820s, 860s and 870s (Newfield, 2013; Haldon et al.,
448 2018; Devroey, 2019). One mid-10th-century source does observe a *hiemps gravissima* (gravest winter) preceding a
449 five-year *fames intolerabilis* (intolerable food shortage) vaguely datable to the early 850s and possibly located in
450 and beyond northern France and Belgium (Newfield, 2013). However, this evidence must be treated with caution
451 given its non-contemporaneity, unsecure dating of events and dramatized tone. It can be noted that the written record
452 of food shortages is certainly incomplete for this period of European history, such that some events of the 850s may
453 have gone undocumented. We may also posit that if extreme weather did not occur when it could affect harvests
454 sufficiently to trigger a serious subsistence crisis, or when society otherwise proved resilient (e.g. through adequate
455 stored reserves), it may have been deemed less relevant for recording.



456

457 **Figure 8: 9th century reports of large subsistence crises (‘famines’, black) and seemingly more circumscribed crises**
458 **(‘lesser food shortages’, orange) recorded in Carolingian sources (Newfield, 2013). Note again that the record of food**
459 **shortages is imperfect: some crises may not have been recorded and the extent and severity of several recorded crises are**
460 **difficult to determine.**

461



462 **Table 1: Climate-relevant events recorded in Irish, Carolingian, Anglo-Saxon, Byzantine, Italian, Iberian, Abbasid and**
 463 **Egyptian sources between 850-858 CE. Locations given reflect where the texts were likely at the time compiled, though**
 464 **the phenomena recorded could have been more widespread. Cases where the phenomena locations are instead given are**
 465 **denoted by *.**

Year CE	Event	Location	Source
850	Flooding	Rio Guadalquivir	<i>Meklach et al. (2021)</i>
850	Food shortage	western Germany	<i>Annals of Fulda</i>
850	Winter flood, excessive summer heat	western Germany	<i>Annales Xanten</i>
851	Low summer flood	Nile (mainly Blue Nile, rising in Ethiopian highlands)	<i>Kondrashov et al. (2005)</i>
852	Excessive heat contributing to a food shortage	northwestern Germany	<i>Annals of Xanten</i>
853	Food shortage	northwestern Germany	<i>Annals of Xanten</i>
854/5	Cold winds, disease	Baghdad	<i>Ibn al-Jawzi</i>
855	Deep snow in late April	* Ireland (unspecific)	<i>Annals of Ulster</i>
855	Frost and frozen lakes (to loadbearing strength)	* Munster, Ireland	<i>Annals of the Four Masters, Fragmentary Annals</i>
855	Large hail	Baghdad	<i>Ibn al-Jawzi</i>
855	Unusual hail and storms	central Germany	<i>Annals of Fulda</i>
855/6	Lakes and rivers frozen	* All Ireland (implied)	<i>Annals of Ulster, Chronicon Scotorum, Annals of the Four Masters, Fragmentary Annals</i>
856	Tempestuous and harsh year	* Ireland (unspecific)	<i>Chronicon Scotorum, Annals of Ulster</i>
856	Severe, dry winter, epidemic	northern France	<i>Annals of St Bertin</i>
857	Lightning kills three persons	* Meath, eastern Ireland	<i>Chronicon Scotorum, Annals of Ulster, Annals of the Four Masters, Fragmentary Annals</i>
857	Great windstorm, destroys trees and lake islands (crannogs)	* Ireland (unspecific)	<i>Annals of Ulster</i>
857	Epidemic	northwestern Germany	<i>Annals of Xanten</i>
858	Epidemic, flood	northern France	<i>Annals of St Bertin</i>
858	Wet autumn, destructive to agriculture and/or fruiting plants	* Ireland (unspecific)	<i>Annals of Ulster</i>
858	Famine	* Ireland (unspecific)	<i>Fragmentary annals</i>
858	Epidemic, heavy rain and snow	Baghdad	<i>Ibn al-Tabarī, Ibn al-Jawzi</i>

466

467 Elsewhere, in Iberia, we read only of significant flooding along the Rio Guadalquivir in 849 and 850 CE (Meklach
 468 et al., 2021), while there are no known reports in Anglo-Saxon, Byzantine, Italian or Iberian sources of anomalous
 469 weather ~853 CE or potentially related societal events that might suggest climate perturbations then. Further east,
 470 however, the scholar Ibn al-Jawzi (writing in the twelfth century, but with access to contemporary sources for our



471 period) wrote that for the year 240 (854/5 CE), a cold wind ‘came out from the land of the Turks and many died
472 from having a cold... the winds continued to Iraq and the people of Samarra and Baghdad suffered from fever and
473 cough and cold.’ Then, in March 855 CE, ‘massive hail’ fell in Baghdad, ‘sized larger than nuts, along with heavy
474 rainfall.’ In the year 244 (858/9 CE) the eyewitness scholar, al-Tabarī recorded that in Syria, ‘pestilence broke out
475 (and the reason for that was) that the air was cold and full of dew, the rainfall heavy... prices rose and there was
476 snow’. When al-Jawzi later wrote up this report in his own history, he added that the snow lasted more than two
477 months (Table 1).

478 A suppression of the East African Monsoon may have been expected with a NH winter eruption of this magnitude
479 (Manning et al. 2017; Oman et al. 2006); however, the extant historical sources do not identify such a happening.
480 Egyptian historical records are silent. The Nilometer recordings of high and low stands of the annual Nile flood at
481 and after the date of the eruption do not appear anomalous, and there are no known incidences of food crisis or
482 famine that we would otherwise expect from unusually low Nile flooding (Hassan, 2007). Only a low flood (the 5th
483 lowest of the 9th century) is recorded in 851 CE (Kondrashov et al., 2005). Given that this would have largely been
484 the product of lessened monsoon rainfall in summer over the Ethiopian highlands, this low Nile cannot be credibly
485 linked to the eruption date of Mt Churchill, even when accounting for a +/- 1 year potential uncertainty that places
486 the potential eruption date as early as winter 851 CE. There are also no sources from the Nubian Nile that suggest
487 the presence of climatic anomalies or societal reaction to them during this time period (Adam Laitar and Giovanni
488 Ruffini, pers. comm.).

489 Chinese historical sources register local and regional weather anomalies and impacts in eastern China in the years
490 following the eruption. Of particular note is a drought in the summer of 852 CE, affecting the Huainan Circuit,
491 comprising some 12 prefectures and 53 counties, and situated between the Huai and the Yangzi rivers. Famine
492 associated with the drought induced migration, with people resorting to wild foods (Zhang, 2004; as per the *New*
493 *Book of Tang*). There is also a record in 854 and 855 CE of a further drought followed by a famine in several
494 counties in Huainan (Chen, 1986; Zhang, 2004). The government intervened with relief measures consisting of tax
495 reductions and food shipments. A devastating flood then occurred in 858 CE and engulfed a large area, including
496 several prefectures along the Grand Canal, in Hebei, Henan and Huainan circuits (Somers, 1979; Chen, 1986;
497 Zhang, 2004). Water then rose several feet, causing massive loss of life. Given its immense geographical area,
498 natural disasters were common on at least local scales at various latitudes across the Chinese landmass, which,
499 coupled with human disruptions, such as banditism and government neglect, often had calamitous social and
500 economic effects. We can therefore again stress that the events of the 850s CE cannot be uncritically linked to the
501 climatic impacts of the Mt Churchill eruption, and when considered in the context of 9th-century Chinese climate
502 history, more severe, widespread and prolonged weather extremes are documented (Yin et al., 2005). However, the
503 reporting of drought in 852, 854 and 855 CE in Huainan (east China) is consistent with expectations of a
504 suppression of East Asian summer monsoon rainfall following a high-latitude Northern Hemispheric eruption (e.g.,
505 Zhuo et al., 2014; Iles and Hegerl, 2015).



506 4. Discussion

507 4.1 Climatic impact of the 852/3 CE Churchill eruption

508 The VEI 6 eruption of Churchill in the winter of $852/3 \pm 1$ CE was amongst the largest eruptions of the Common
509 Era and dispersed ash eastwards over a distance of 7,000 km. Despite its large magnitude, on the basis of sulfate
510 deposition in Greenland ice cores, the eruption appears to have had only moderate climate forcing potential: the
511 SAOD perturbation is concentrated in the NH and there are four other volcanic events in the 9th century that have
512 larger global mean SAOD. The 852/3 CE Churchill eruption therefore contributes to the known examples of large
513 magnitude Common Era eruptions that are associated with moderate atmospheric sulfate burdens as reconstructed
514 from ice-cores (Sigl et al., 2013, 2014, 2015), such as Taupo 232 ± 10 CE (Hogg et al., 2012; Hogg et al., 2019);
515 Changbaishan 946 CE (Sun et al., 2014; Oppenheimer et al., 2017); and Long Island 1661 ± 10 CE (Blong et al.,
516 2018).

517 Despite the moderate climate forcing potential of the 852/3 CE Churchill eruption estimated from ice core sulfate
518 records, there is evidence for a strong NH cooling associated with 853 CE. Tree-ring temperature reconstructions
519 show temperature declines centred on summer 853 CE with a peak magnitude of around -0.8°C . In terms of 3-year
520 mean NH summer temperature, the 853-856 CE period is the 11th coldest period between 500 and 2000 CE
521 (Appendix G). Climate model simulations which incorporate estimates of the stratospheric sulfate aerosol forcing
522 based on ice core records produce NH summer land temperature anomalies of around -0.3°C , while individual
523 ensemble members display cooling as large as -0.8°C , comparable to the tree ring-based estimates. The model
524 simulations thus suggest that the tree-ring-derived cooling is explainable as a result of the combined effects of
525 internal climate variability and volcanic aerosol forced cooling. The spatial patterns of the summer temperature
526 decrease generally agree with the tree-ring-based reconstructions and the ensemble model simulations. For example,
527 the growing season cooling registered in the NH tree-ring records is initially pronounced in western and central
528 Europe and Scandinavia, with colder conditions in Alaska, which generally aligns with the spatial patterns of
529 cooling found in the ensemble means of climate simulations. The peak summer cooling in the tree-ring records in
530 853 CE is influenced by a shift to cold conditions central Asia and Siberia. The cooling in these regions is also
531 expressed in the model simulations in the summers of 853 and 854 CE, although with reduced amplitudes of
532 temperature variability compared with the tree-ring temperature records. Strong cooling in central Asia and Siberia
533 has been reconstructed from tree-rings in the years following many other large eruptions in the Common Era, such
534 as the assumed Mount Asama eruption and unidentified volcanic eruptions in 1109 CE (Guillet et al., 2020), the
535 Mount Samalas eruption in 1257 CE (Guillet et al., 2017), an unidentified eruption in 1453 CE (Stoffel et al., 2015;
536 Abbott et al., 2021) and the Huaynaputina eruption in 1601 CE (White et al., in review).

537 In some respects, however, the spatial patterns differ between the climate model simulations and the tree-ring
538 reconstructions. In particular, the persistent cool conditions in central Asia and Siberia in 855 CE are only found in
539 the tree-ring-based reconstructions. These deviations (changes in temperature amplitudes and in spatial patterns) are



540 expected as the ensemble means of the simulations focus on the signal of the volcanic eruption by reducing internal
541 climate system variability. In contrast the tree-ring-based reconstruction contains both internal variability and the
542 potential forcing signal of the eruption and/or other external drivers. Therefore, the reconstructed cooling in Asia
543 and Siberia in 855 CE is potentially related to internal variability of the climate, such as changes in the large-scale
544 atmospheric circulation rather than being externally forced by the Churchill eruption.

545 The reconstructed climatic cooling peak in 853 CE aligns with the eruption date of the winter 852/3 CE Churchill
546 eruption but the timing of the start of this tree-ring-inferred cooling trend begins in summer of 851 CE, thereby
547 predating the eruption (and its associated age uncertainty). However, the magnitude of the temperature decline in
548 summer 851 CE is within the range of natural temperature variability and it is not until the summers of 852 and 853
549 CE when temperatures exceed the range of natural variability. The modelled climate scenario cooling occurs later in
550 853 CE, with widespread cooling present in summer 854 CE and winter 854 CE. The results from the tree-ring-
551 based temperature reconstructions preclude attribution of the climatic cooling solely to the Churchill eruption, but
552 the eruption timing clearly corresponds with cooling as registered in both reconstructed and simulated approaches.
553 These findings therefore suggest that the winter 852/3 CE Churchill eruption exacerbated a naturally occurring cold
554 period. This is supported by the decadal-scale step changes in temperatures recorded in the tree-ring-based
555 reconstructions (Fig. 4a) and NGRIP1 $\delta^{18}\text{O}$ reconstructions (Fig. 6, Appendix J) prior to and after 852/853 CE.

556 Hydroclimate changes driven by volcanic eruptions are less clearly defined than those of temperature, partly due to
557 the higher degree of variability in precipitation and the small changes in atmospheric moisture associated with the
558 magnitude of temperature change often associated with volcanic-cooling. For example, the Clausius–Clapeyron
559 relationship predicts that the water-holding capacity of the atmosphere decreases by approximately 7% for every
560 1°C cooling (Held and Soden, 2006). Therefore, moisture changes associated with the 852/3 CE Churchill eruption
561 would be expected to be in the order of ca. <5%. Some observational and modelling studies have, however, reported
562 a reduction in global precipitation following explosive volcanic eruptions (e.g. Robock and Liu, 1994; Iles et al.,
563 2013). Evidence to support a change in precipitation driven by the 852/3 CE eruption is lacking: no statistical
564 changes were detected in NH precipitation variability during the 853 CE eruption period in this study and spatial
565 patterns of precipitation reconstructed from climate modelling and tree-rings are inconsistent, suggesting that
566 internal climate system variability dominates. There is also no evidence from the palaeoenvironmental
567 reconstructions to support hydrological changes on multidecadal time scales as changes in the peatland water depths
568 differ spatially and temporarily and most records present longer centennial-scale changes that do not correspond
569 with the eruption date.

570 The climate forcing of the 852/3 CE Churchill eruption derived from existing ice-core records and used in the
571 climate model simulations is the current best estimate. Uncertainty in the stratospheric aerosol forcing (as shown in
572 Fig 3b) is not incorporated into the model simulations as e.g., was done by Timmreck et al. (2021). Furthermore,
573 additional forcing factors have not been explicitly taken into account. In particular, this explosive eruption is
574 characterised by high chlorine concentrations in the ice-cores (Fig. 2) and a very extensive ash-cloud across the NH



575 mid to high latitudes, suggesting large atmospheric loadings. Emissions of halogens and ash have the potential to
576 influence climate but their climate forcing potential is poorly constrained and so they remain unaccounted for in the
577 EVA and EVA_H forcing time series, as well as in the CESM simulations. The injection of a large quantity of
578 halogens along with sulfur by the 852/3 CE eruption may have modulated the impact on surface temperatures: some
579 model studies suggest coemission of halogens may intensify or prolong the volcanic cooling (Wade et al. 2020,
580 Staunton-Sykes et al. 2021), although contrasting model results suggest the effect may be model or event dependent
581 (Brenna et al. 2020). The influence of ash on radiative forcing is currently unclear. For example, recent observations
582 for the Kelud 2014 eruption suggest that ash exerted a radiative forcing of -0.08 W/m^2 three months after the
583 eruption (Vernier et al. 2016), even though the volcano erupted only $0.5 \pm 0.2 \times 10^{11} \text{ kg}$ of ash (Maeno et al. 2019,
584 Aubry et al., 2021). In comparison, we found that the Churchill eruption erupted $4.9 \times 10^{13} \text{ kg}$ ($3.9\text{--}6.1 \times 10^{13} \text{ kg}$) of
585 ash, which might suggest a potentially strong radiative forcing from ash that is unaccounted for in our modelling.
586 However, the short lifetime of ash in the atmosphere makes it questionable whether the associated forcing would
587 persist long enough to significantly affect surface temperature and tree-ring growth. Furthermore, the co-injection of
588 ash with sulfur could likely reduce the radiative forcing associated with sulfate aerosol since ash particles uptake
589 sulfur dioxide, thereby reducing its lifetime (Zhu et al. 2020).

590 **4.2 Climatic-Societal impacts of the 852/3 CE Churchill eruption**

591 The White River Ash east (WRAe) deposit from the 852/3 CE Churchill eruption has reported thicknesses of 50–80
592 m proximal to Mount Churchill, and visibly extends in an easterly direction $>1,300 \text{ km}$ from the source (e.g.,
593 Richter et al., 1995; Lerbekmo 2008; Patterson et al., 2017). The considerable ash fallout synonymous with this
594 eruption had lasting environmental and societal consequences for regions proximal to the source, driven primarily
595 by the physical and chemical impacts of emissions from the eruption. Known impacts include changes in vegetation
596 and wetland ecology (e.g. Rainville, 2016; Payne and Blackford, 2008; Bunbury and Gajewski, 2013) and
597 displacement of local human populations (e.g. Kristensen et al., 2020; Hare et al., 2004; Mullen, 2012).

598 Historical records gleaned from a wide range of sources across Europe, Africa and Asia provide an opportunity to (i)
599 assess the extent to which the 852/3 CE Churchill eruption had distal societal consequences, (ii) corroborate or
600 critique results from the modelled and tree-ring-based climate scenarios around the time of the Churchill eruption,
601 and (iii) identify any evidence of extreme weather conditions that is not registered in the paleoenvironmental
602 reconstructions, such as severe winters. European historical records spanning the 850s document some anomalous
603 conditions, albeit fewer extreme weather events and associated crises than in other decades of the 9th century (Fig.
604 8). Food shortages and extreme weather were reported shortly before and after the 852/3 CE eruption in western
605 Germany; a severe subsistence crisis may have also occurred in nearby northern France and Belgium that set in
606 during the eruption year or shortly thereafter. Tree-ring reconstructions show that the growing season in 852 CE was
607 particularly cold in Europe, with temperature declines of -2°C or more in northwest Europe, and simulated
608 temperatures also show a temperature decline, albeit to a lesser magnitude (ca. -0.2°C). The cause of the crisis in
609 Germany in 853 CE is not detailed in the sources, nor are weather extremes observed that would corroborate the



610 inferred temperature anomaly. An extreme winter is identified as the cause of a food shortage reported in northern
611 France and Belgium in the early 850s, but the dates of the winter and the food shortage are not certain. It is notable
612 that a particularly sustained effort to record natural phenomena (including extreme weather) was undertaken in Irish
613 monasteries in the ninth and adjacent centuries (McCarthy and Breen, 1997; McCarthy, 2008), perhaps making it
614 more likely that unusual weather would be recorded here even in the absence of major societal impacts. Moreover, a
615 survey of 1,219 years of reporting of severe cold (mainly in winter) in Irish annals has revealed a repeated link to
616 explosive volcanism as registered in elevated Greenland sulphate, such that the medieval Irish may have been
617 particularly acute observers of volcanic winter-season impacts (Ludlow et al., 2013). However, there are no reported
618 extreme weather events in Ireland in the early 850s. Repeated reports of extreme cold occur from April of 855 CE to
619 winter 855/6 CE for Ireland occur amidst a return to average climatic conditions in the tree-ring reconstructions and
620 modelled climate scenarios for western Europe. Elsewhere, in the area of Huainan, China, drought is recorded in 852
621 CE, 854 CE and 855 CE and is consistent with the expected impacts of high-latitude Northern Hemispheric volcanic
622 eruptions on the East Asian summer monsoon (e.g., Zhuo et al, 2014; Iles and Hegerl, 2015). There is, therefore,
623 some agreement between the historical records and reconstructed and modelled climate, but not uniformly so
624 between 851-855 CE.

625 The pollen records are insufficiently resolved to identify sub-decadal anomalies or extreme weather events, but they
626 provide a useful longer-term perspective on societal adaptation to climate variability. Precise comparisons of the
627 pollen assemblages between sites are facilitated by the presence of WRAe, which dispels any chronological
628 uncertainty with respect to the timing of changes in land-use. The pollen records clearly show spatially complex
629 patterns in the extent and intensity of land-use, implying that changes in human activity around this time were not
630 driven merely by responses to changing environmental conditions. Rather, it would seem that any observed cultural
631 shifts around this time reflect an interplay of social, economic and political factors.

632 **4.3 Transatlantic comparisons of terrestrial hydroclimate change in the Medieval Period**

633 The MCA is commonly characterised as a warm period ca. 950–1250 CE (Mann et al., 2009), with dry conditions in
634 Europe and North America (e.g. Büntgen and Tegel, 2011; Ladd et al., 2018; Marlon et al., 2017). There is,
635 however, considerable spatial variability in the timings of the MCA onset and peak warmth (e.g. Neukom et al.,
636 2019) as well as hydroclimatic expressions (e.g. Shuman et al., 2018). In order to assess regional variability in
637 terrestrial MCA hydroclimate across northeastern North America and western Europe, this study provides
638 chronologically precise hydroclimatic comparisons facilitated by the detection of the WRAe isochron in our
639 peatland archives as well as the NGRIP1 ice core, which acts as a chronological tie point between the
640 palaeoenvironmental reconstructions. Comparisons of our eleven peatland records show that there is no consistent
641 multidecadal-scale hydrological response associated with the MCA; rather hydrological conditions are variable both
642 within and between records. There are also no clear temperature trends associated with the MCA detected in the
643 NGRIP1 $\delta^{18}\text{O}$ record (Fig. 6): temperatures are elevated in central Greenland during the 10th century but these are
644 not sustained during the remainder of the medieval period, which is generally characterised by cooler, fluctuating



645 temperatures. These findings suggest that there is no clear climatic expression of the MCA in the North Atlantic
646 region.

647 The environmental reconstructions presented in this study highlight the heterogeneous and time-transgressive nature
648 of the reconstructed MCA hydroclimate change. For example, a dry shift, which may be typical of a MCA climate
649 response, began ca. 900 CE in northern Nova Scotia and some records in Newfoundland, and corresponds with a
650 change to warmer conditions in central Greenland. However, the onset of drier conditions is delayed by ca. 100
651 years in more south-westerly sites in Nova Scotia and Maine as well as on the east coast of the North Atlantic in
652 Ireland. In addition, all peatland records contain temporary wet shifts that occur prior to the MCA ca. 700-850 CE,
653 which corresponds with a period of generally colder temperatures in central Greenland as reconstructed from the
654 NGRIP1 $\delta^{18}\text{O}$. The timings and extent of the wet shifts vary, however, between peatland records with no clear
655 spatial patterns to provide insight into the climate forcing mechanism driving this change. NGRIP1 records another
656 more abrupt and pronounced temperature decrease ca. 1000–1050 CE, the time of which corresponds to a temporary
657 wet shift in several peatland records from Ireland, Newfoundland, Nova Scotia and Maine. However, once again the
658 timing and extent of these wet shifts vary between reconstructions. The chronological precision afforded by the
659 presence of the WRAe isochron in climate reconstructed presented in this study therefore conclusively demonstrates
660 that the differences in the timings of hydroclimatic change between records reflect a true difference in peatland
661 responses to environmental conditions and are not a feature of chronological uncertainty generated from the age-
662 depth modelling process.

663 Here we have reported the dominant peatland hydroclimatic patterns that are supported by multiple regional
664 peatland records; however, some differences exist between proximal reconstructions, such as the clusters of three
665 peatland records developed within ca. 10 km in eastern Newfoundland and two records within ca. 110 km in Maine.
666 The differences in hydroclimate at such local levels in Newfoundland may reflect the degree of spatial hydroclimate
667 variability during this period, but also may be exacerbated by autogenic-driven peatland responses such as enhanced
668 peat accumulation under warmer MCA climates that would drive an apparent lowering of the water table (e.g.
669 Swindles et al., 2012). The divergence between the hydroclimate reconstructions obtained from the Maine peatlands
670 is likely influenced by a fire disturbance event at one of the sites, Saco Heath, which created a substantial hiatus in
671 peat accumulation in some areas of the site (Clifford and Booth, 2013). Whilst the Saco Heath record presented here
672 appears less impacted by the fire, there is a high degree uncertainty in the hydroclimate reconstruction between ca.
673 1000-1250 CE when the accumulation rate slows, which may reflect a temporary hiatus (Figure 6; Appendix D).
674 The development of more palaeoenvironmental reconstructions from sites containing the WRAe, particularly in
675 locations such as Maine and western Europe, will be useful to investigate further MCA trends further.

676 5. Conclusions

677 The winter 852/3 \pm 1 CE Churchill eruption was one of the largest magnitude volcanic events of the first
678 millennium. Tree-ring temperature reconstructions show a NH summer temperature anomaly of around -0.8°C in



679 853 CE, and the corresponding 3-year mean temperature anomaly ranks as the 11th coldest over the 500-2000 CE
680 period (Appendix G). On the other hand, the reconstructed climate forcing potential (i.e. atmospheric sulfate burden)
681 of this eruption derived from ice core records is moderate, smaller than that associated with the 1991 Pinatubo
682 eruption. This apparent mismatch between forcing and response is, we find, explainable as resulting from the
683 combined impact of natural climate variability and volcanic aerosol forcing. Climate model simulations driven by
684 reconstructed aerosol forcing show an ensemble mean response of -0.3°C , but individual ensemble members that
685 show cooling of up to -0.8°C comparable to the tree-ring reconstructions. Support for the correspondence of the
686 eruption with a naturally occurring cool period is provided by the timings of the cooling trend reconstructed by the
687 tree-rings, which begins in summer 851 CE and therefore predates the winter 851/2 to winter 853/4 CE age
688 uncertainty of the eruption, and the seasonal-scale NGRIP1 temperature reconstruction (Appendix J). The simulated
689 temperature response of the eruption may also be underestimated, because the forcing potential models do not
690 account for the potential role of halogens or volcanic ash, both of which show high atmospheric abundances after the
691 eruption. Further research in combined sulphur, halogen and ash modelling and better ice-core constraints about
692 their atmospheric loadings are therefore required to provide more holistic understandings of potential ash-rich
693 volcanic impacts on climate and society.

694 Areas proximal to Mount Churchill experienced widespread and prolonged ecological, environmental and societal
695 changes attributed to the eruption emissions, but there is no evidence of multidecadal-scale climatic response
696 preserved in distal palaeohydrological records from the North Atlantic region that are precisely temporally linked by
697 the 853 CE Churchill WRAe isochron. Pollen records of vegetation change and human activity from Ireland linked
698 by the WRAe isochron also provide no evidence to support long-lasting societal responses in Ireland associated with
699 the eruption. Evidence of short-term societal impacts in Europe from the 852/3 CE Churchill eruption remains
700 equivocal: some historical records from Ireland and Germany, and possibly northern France and Belgium, report
701 harsh winter conditions and food shortages within the age uncertainties of the eruption but similar events were
702 reported outside of the eruption period and were not unknown in the 9th century. The 852/3 CE Churchill eruption
703 therefore exemplifies the difficulties of identifying and confirming volcanic impacts on society even when only a
704 small eruption age uncertainty exists.

705 The presence of the WRAe isochron in peatlands in northeastern North America and western Europe assists with
706 comparisons of hydroclimatic reconstructions during the Medieval Climatic Anomaly, often defined as a period of
707 globally increased temperatures between 950–1250 CE (Mann et al., 2009). Reconstructed hydroclimate conditions
708 in 853 CE vary, highlighting leads and lags in the terrestrial responses to environmental change that may otherwise
709 be considered contemporaneous without the temporal precision provided by the WRAe. This study shows a lack of a
710 consistent terrestrial response to MCA climate change in the North Atlantic region; rather the MCA time period is
711 characterised by time-transgressive and heterogenous hydroclimatic conditions. These findings contribute to a
712 growing body of research that cautions against the application of the globally defined MCA characteristics when
713 interpreting individual records of palaeoenvironmental change and ultimately questions the detectability of a
714 coherent MCA climate signature.



715 **Appendices**

716 **Appendix A: Additional methodological information to support the forcing potential reconstructions (Section**
717 **2.2)**

718 The EVA (eVolv2k) reconstruction (Toohey and Sigl, 2017) is the recommended volcanic forcing dataset for
719 climate model simulations of the Paleoclimate Modeling Intercomparison Project (PMIP, Jungclaus et al., 2017;
720 Kageyama et al., 2018). The EVA reconstruction uses volcanic stratospheric sulfur injection estimates derived from
721 sulfate deposition from an extensive bipolar array of ice cores (Sigl et al. 2015), which are then converted into an
722 SAOD time series using the idealized, scaling based aerosol model Easy Volcanic Aerosol (EVA, Toohey et al.,
723 2016). The global mean radiative forcing (RF) time series is estimated from the SAOD using the following
724 relationship from Marshall et al. (2020):

725
$$RF = -19.2 \times (1 - e^{-SAOD}) \quad (1)$$

726 where RF is in $W m^{-2}$.

727 **Appendix B: Additional methodological information to support the climate model simulations (Section 2.3)**

728 An initial condition ensemble simulation was created using the Community Earth System Model version 1.2.2
729 (CESM), consisting of 20 ensemble members. CESM is a state-of-the-art fully coupled Earth system model
730 composed of atmosphere, land, ocean, and sea ice components. To generate the ensemble members, initially a
731 seamless transient simulation was run from 1501 BCE (Kim et al., 2021) with time-varying orbital parameters
732 (Berger, 1978), TSI (Vieira et al., 2011; Usoskin et al., 2014, 2016), GHG (Joos and Spahni, 2008; Bereiter et al.,
733 2015), and volcanic forcing from the HolVol v.1.0 (Sigl et al., 2021) and eVolv2k (Toohey and Sigl, 2017)
734 databases. The necessary prescribed spatial-temporal distribution of volcanic sulfate aerosol for the simulation is
735 generated using the Easy Volcanic Aerosol Model (EVA, Toohey et al., 2016) and following the same procedure
736 employed by McConnell et al. (2020) and Kim et al. (2021). In the procedure, the EVA-generated spatio-temporal
737 distribution of sulfate was first converted to volcanic aerosol mass to be readable by CESM. This distribution of
738 volcanic aerosol mass in CESM was scaled up by 1.49 to reconcile CESM and EVA atmospheric responses to the
739 1991 Pinatubo eruption. Then, the transient simulation was branched off at 845 CE and a small perturbation was
740 introduced at the first time step in the atmosphere. The 20 ensemble members were run from this point until 859 CE.
741 During this 14 year period, no other volcanic eruptions were included except the 852/853 CE Churchill eruption.

742 Mann-Whitney U-test was used to test the statistical significance of changes in temperature and precipitation after
743 the Churchill eruption. The null hypothesis of a Mann-Whitney U-test test states that the two datasets share the same
744 statistical distribution derived from the same population. In this study, the distributions of the temperature and
745 precipitation anomalies after Churchill eruption (853, 854 and 855 CE individually) derived from all ensemble
746 members were compared to those of the 845–852 CE pre-eruption period ensemble. We assume that changes in
747 temperature and precipitation after the eruption are statistically significant if the null hypothesis of the Mann-
748 Whitney U-test test is rejected at 5% confidence level.



749 **Appendix C: Additional methodological information to support the NH tree-ring summer temperature**
750 **reconstructions (Section 2.4)**

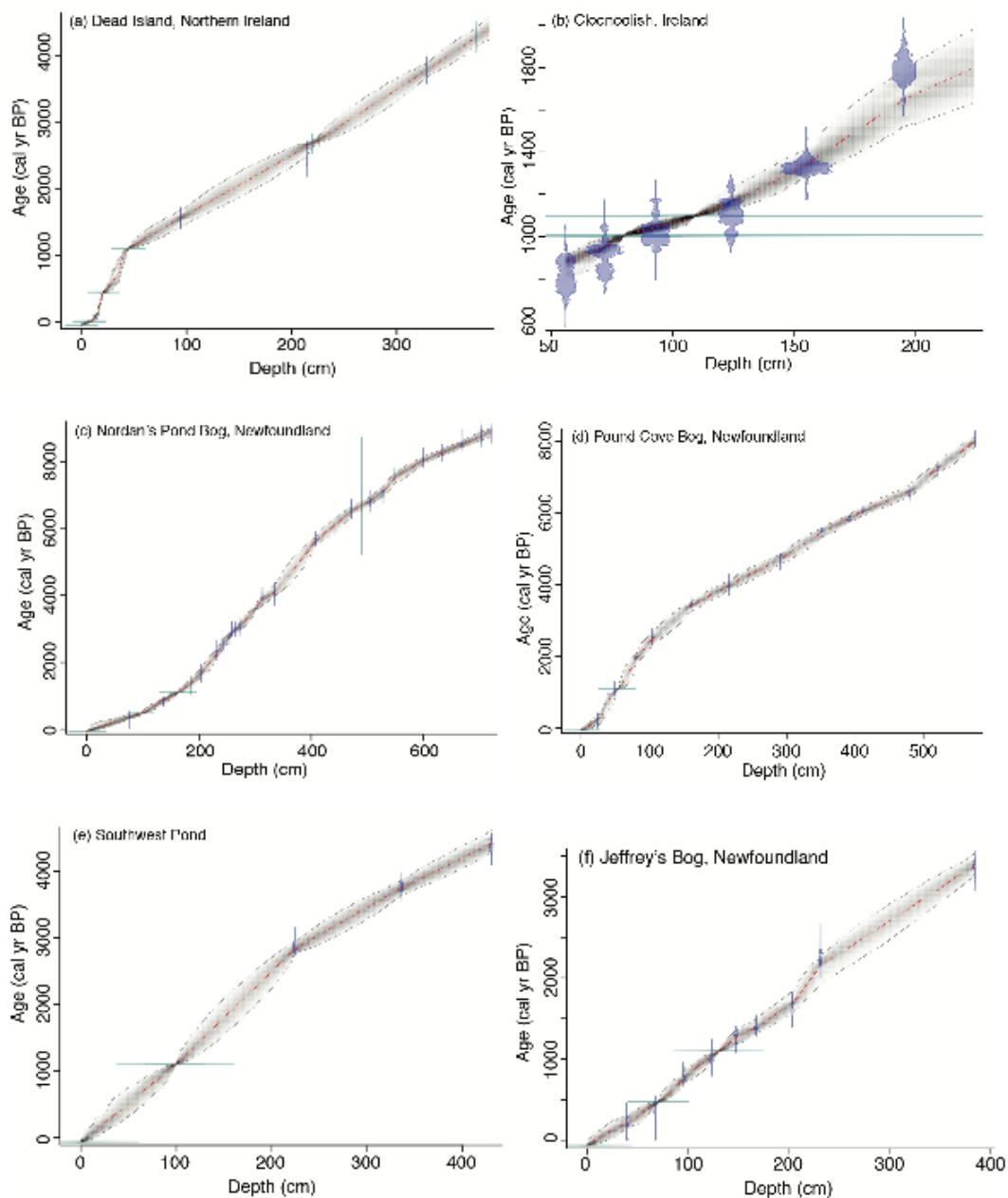
751 We employed a principal component regression (PCR) to reconstruct NH JJA temperature anomalies (with respect to
752 1961–1990) from tree-ring records. We coupled this PCR with a bootstrap random sampling approach to quantify the
753 robustness of our reconstruction and to estimate confidence intervals of reconstructed JJA temperatures. To account
754 for the decreasing number of records available back in time, we combined the PCR with a nested approach. In total,
755 our reconstruction is based on 23 subsets of tree-ring chronologies or nests. The earliest and most recent nests span
756 the periods 500–551 and 1992–2000 CE, respectively. The most replicated nest (1230–1972 CE) includes 25
757 chronologies. For each nest, we reduced the proxy predictors matrix to principal components (PCs) using a Principal
758 Component Analysis (PCA). PCs with eigenvalues >1 were included as predictors in multiple linear regression models
759 calibrated on JJA temperature (1805–1972 CE) extracted from the Berkeley Earth Surface (BEST) dataset
760 (<http://berkeleyearth.org/data/>). We assessed the robustness of each model using a split calibration–verification
761 procedure using a bootstrap approach repeated 1,000 times. We computed the final reconstruction of each nest as the
762 median of the 1,000 realizations. The final 500–2000 CE reconstruction combines the 23 nests with their mean and
763 variance adjusted to be identical to the 1230–1972 CE most replicated one. To place the summer temperature
764 anomalies within the context of climate variability at the time of major volcanic eruptions, we removed longer
765 timescale variations by filtering the final reconstruction, which involved calculating the difference between the raw
766 time series and the 31-yr running mean.

767 The target field (predictand) used for the reconstruction is the BEST JJA gridded temperature dataset ($1^\circ \times 1^\circ$ latitude-
768 longitude grid). We divided the NH into 11 subregions defined according to the spatial distribution of the 25 tree-ring
769 records and their correlation. Chronologies were grouped in the same subregion when their correlation coefficients
770 over their overlapping period exceeded 0.3. Only one chronology was included in the Quebec, Western and Central
771 Europe, Siberia - Taymir, Siberia - Yakutia, and China - Qilian Mountains subregions. In these clusters, we used an
772 ordinary least square regression to reconstruct JJA temperatures. In the other subregions such as Western and Central
773 Europe – which includes five TRW and MXD records – we used the nested PCR approach (see above) to reconstruct
774 gridded summer temperature anomalies. Based on this approach, we reconstructed robust temperature anomalies back
775 to 500 CE for 3486 NH grid points.

776

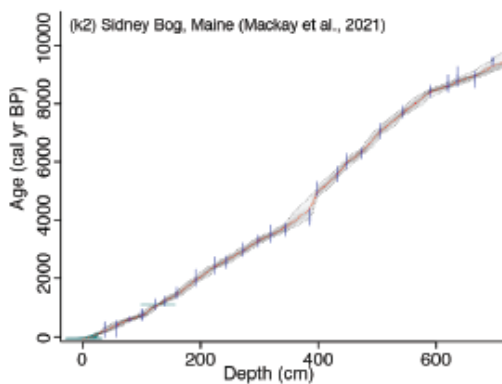
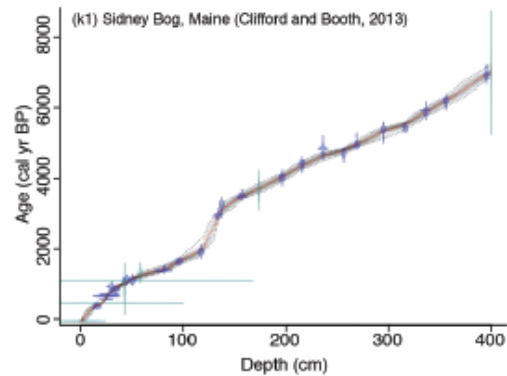
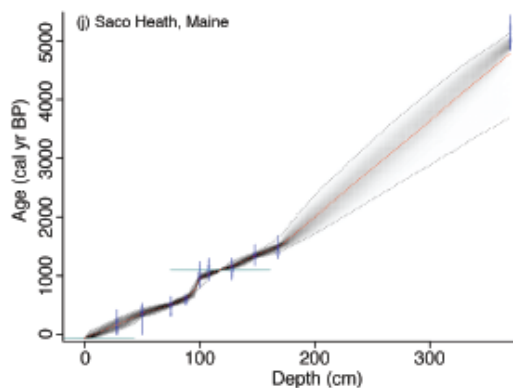
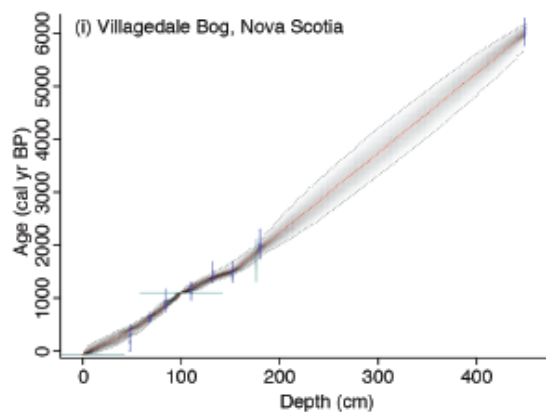
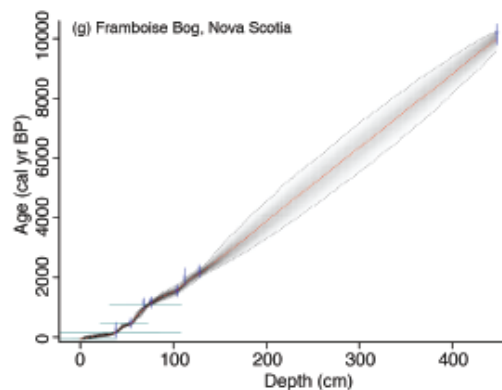
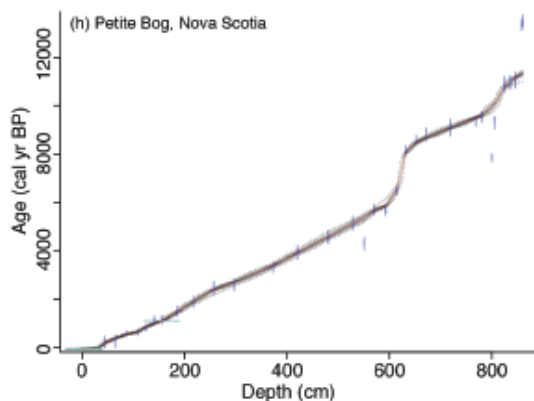


777 **Appendix D: Peatland chronologies**

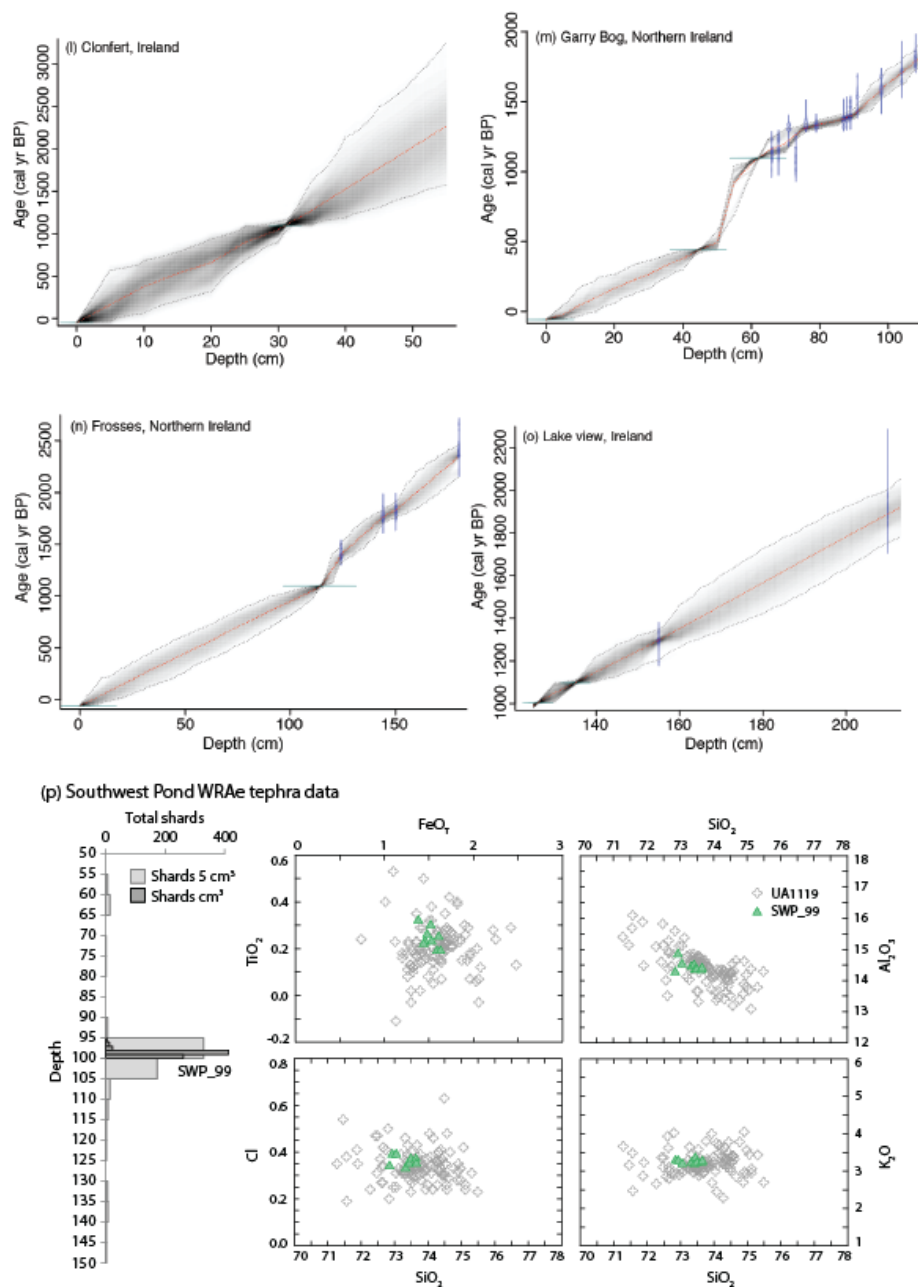


778

779



780

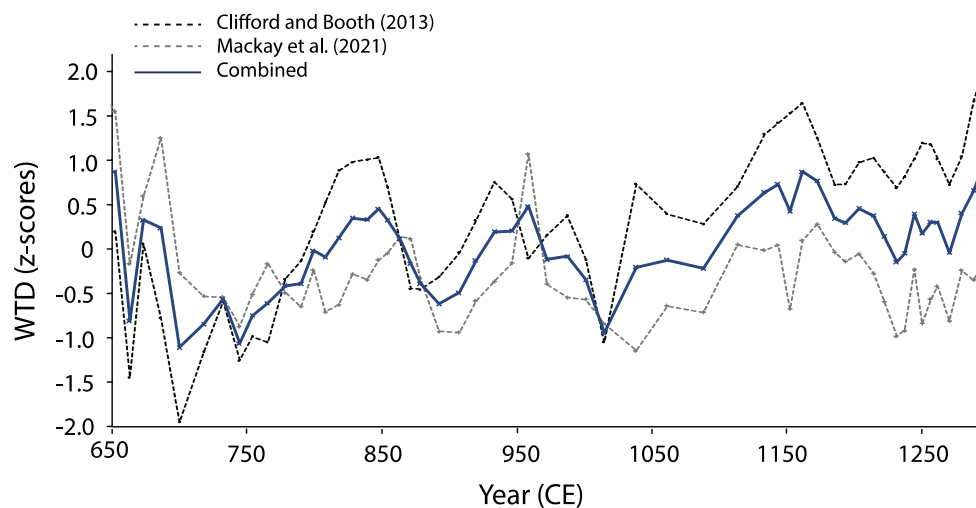


781
782
783
784
785

Fig. D1: (a-o): Core chronologies (Sup. Fig. 1a-o) were developed using Bayesian analysis within the R package “BACON” (Blaauw and Christen, 2011) based on ¹⁴C dates (calibrated using NH IntCal20 calibration Curve (Reimer et al., 2020)) and tephrochronologies. (p): Shard counts and major-minor element glass compositions for the WRAe in Southwest Pond Bog. Comparative glass electron probe microanalysis data (UA1119) is taken from Jensen et al. (2014).



786 **Appendix E: Composite testate amoebae-inferred peatland water table record from Sidney Bog, Maine**

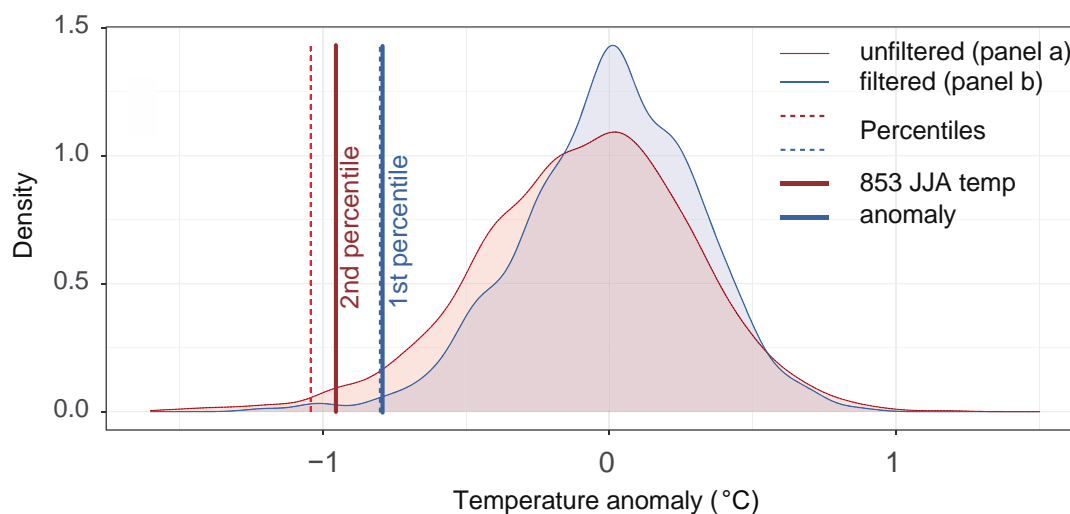


787

788 **Fig. E1: Composite WTD record for Sidney Bog, Maine, USA based on testate amoebae assemblage data obtained from**
789 **two cores obtained from different coring location on the peatland (Clifford and Booth, 2013; Mackay et al., 2021). Testate**
790 **amoebae water table depth (WTD) reconstructions were obtained using the tolerance-downweighted weighted averaging**
791 **model with inverse deshrinking (WA-Tol inv) from the North American transfer function of Amesbury et al. (2018). To**
792 **produce the composite record, the chronological resolution of the Clifford and Booth (2013) WTD record has been**
793 **increased to the same resolution as the Mackay et al. (2021) record using linear interpolation between chronological**
794 **adjacent WTD values. The composite record then presents the average WTD of the interpolated Clifford and Booth**
795 **(2013) and the Mackay et al. (2021) reconstructions.**
796



797 **Appendix F: Tree-ring inferred NH summer temperature anomalies**



798
799
800
801
802
803

Fig. F1: Distributions of JJA temp. anomalies in the unfiltered (blue) and filtered (red, 31 yr-mov. av. Filter) 500-2000 CE, NH reconstructions. Blue and red vertical dotted bars indicate the 1st percentile of the filtered and the 2nd percentile of the unfiltered reconstructions, respectively. Blue and red vertical lines show the cooling observed in 853 CE in the filtered and unfiltered reconstructions, respectively.



804 **Appendix G: Eruption information for tree-ring inferred coldest years between 500–2000 CE**

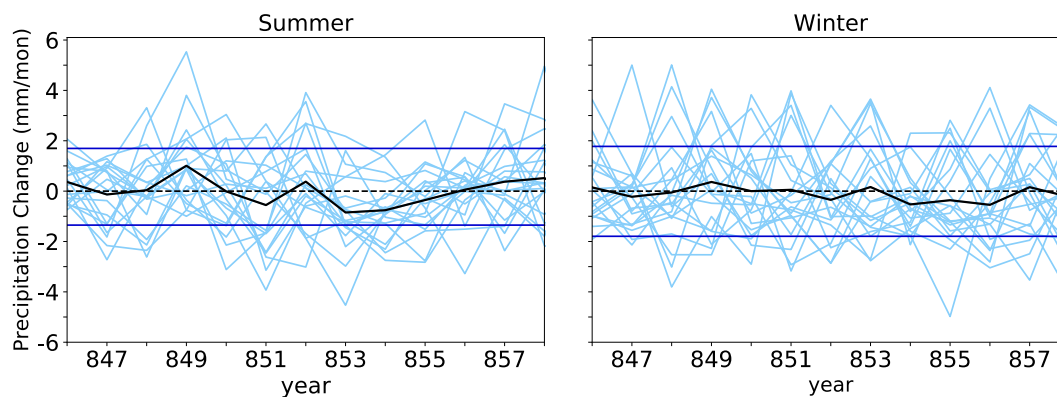
805 Table G1: Top 30 coldest years during the period of 500–2000 CE based on tree-ring temperature anomalies filtered
 806 using a 3-year mean and corresponding eruption information for proximal calendar years. Eruption dates and volcanic
 807 stratospheric sulfate injection (VSSI) estimates taken from the eVolv2k reconstruction (Toohey and Sigl, 2017),
 808 representing the most immediate preceding eruption in the data set. Black = eruption occurred within 2 years of the
 809 coldest reported year; grey = eruption occurred more than 2 years before the coldest reported year.

Rank	Year (CE)	Temperature anomaly	Preceding eruption	VSSI	Time difference (eruption year – cold year)
1	536	-1.40	536 UE	18.8	0
2	627	-1.25	626 UE	13.2	-1
3	1601	-1.25	Huyaniputina 1600	19.0	-1
4	1783	-1.21	Laki 1783	20.8	0
5	1453	-1.09	1453 UE	10.0	0
6	1109	-1.02	1108 UE	19.2	-1
7	1032	-0.95	1028 UE	7.8	-4
8	1259	-0.86	Samalas 1257	59.4	-2
9	800	-0.81	800 UE	2.5	0
10	1463	-0.74	1458 UE	33.0	-5
11	853	-0.71	Churchill 852/853	2.5	-1/0
12	1816	-0.71	Tambora 1815	28.1	-1
13	979	-0.69	976 UE	6.2	-3
14	1833	-0.69	1831 Babuyan	13.0	-2
15	1589	-0.65	Colima 1585	8.5	-4
16	1699	-0.64	1695 UE	15.7	-4
17	1641	-0.62	1640 Parker	18.7	-1
18	637	-0.57	637 UE	1.7	0
19	903	-0.54	900 UE	5.6	-3
20	1459	-0.53	1458 UE	33.0	-1
21	1677	-0.52	1673 UE	4.7	-4
22	1697	-0.44	1695 UE	15.7	-2
23	639	-0.35	637 UE	1.7	-2
24	541	-0.34	540 UE	31.9	-1
25	543	-0.32	540 UE	31.9	-3
26	1835	-0.31	Cosiguina 1835	9.5	0
27	1643	-0.29	1640 Parker	18.7	-3
28	546	-0.26	540 UE	31.9	-6
29	538	-0.25	536 UE	18.8	-2
30	640	-0.07	637 UE	1.7	-3

810

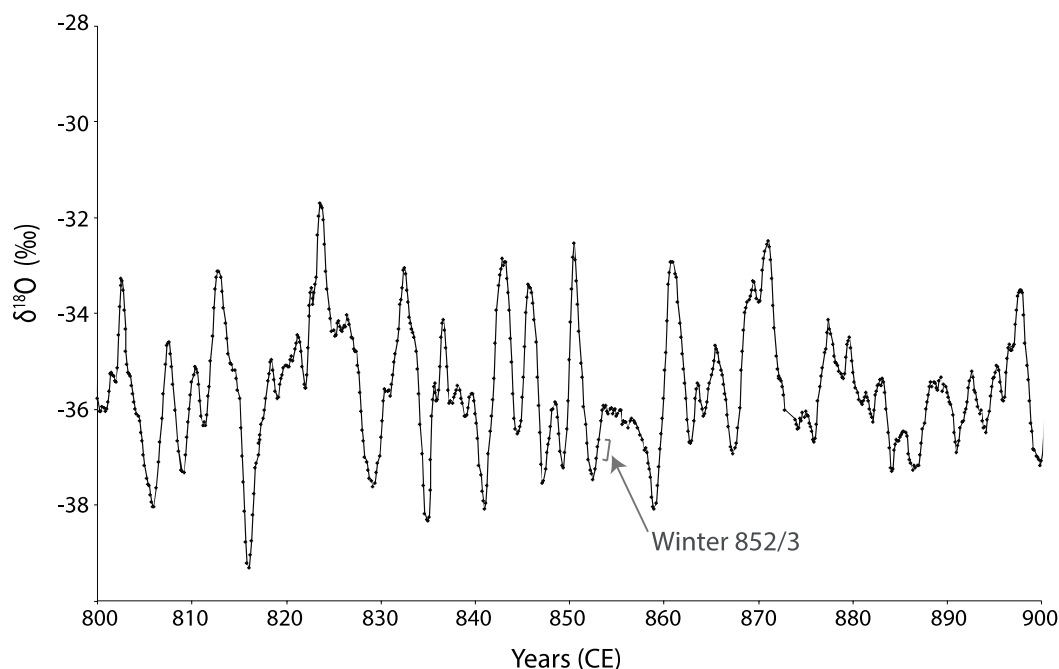


811 **Appendix H: Climate model simulations of NH summer and winter precipitation anomalies between 856-858**
812 **CE**



813
814 **Fig. H1:** The spatially-averaged NH extratropical (15° – 90°N latitudes) precipitation anomalies from 20 ensemble
815 simulations for summer (JJA) and winter (DJF) in light blue lines. The thick black lines indicate the ensemble means and
816 the horizontal blue lines represent one standard deviation from the ensemble means of the 845 – 852 CE pre-eruption
817 period.

818 **Appendix J: NGRIP1 $\delta^{18}\text{O}$ isotopes temperature reconstruction (9th century)**



819

820 **Fig. J1:** NGRIP1 $\delta^{18}\text{O}$ isotopes temperature reconstruction (Vinther et al., 2006), plotted on NS1-2011 chronology (Sigl et
821 al., 2015). Warmer (colder) temperatures are represented by higher (lower) $\delta^{18}\text{O}$ values. The eruption age estimate for the
822 852/3 CE Churchill eruption is denoted.



823 **Author contributions**

824 HM, GP and BJ were responsible for the conceptualization and design of the project. HM, MA, AM, AB and GS
825 conducted the testate amoebae analyses as well as the associated data analysis and interpretation. HM and MA
826 conducted the testate amoebae analyses as part of projects supervised by PDMH, PGL and DC. RB and HM created
827 the Sidney Bog composite testate amoebae record. GP and LCM designed and conducted the Irish pollen and tephra
828 analysis for the Irish sites (exception of Dead Island record, tephrochronology by GS). TA and MT designed the
829 forcing potential analyses, which were conducted by TA. MSigl analyses the ice-core chronologies and associated
830 data. BJ and MB designed the eruption volume estimate and magnitude analyses, which were conducted by MB. WK
831 and CR designed the climate model simulation analyses, which were conducted by WK. CC and MStoffel designed
832 the tree-ring temperature reconstruction analyses, which were conducted by CC. KJA designed and analysed the tree-
833 ring drought reconstructions. JM, TPN, NDC, FL, CK and ZY analysed the historical records. HM, KLD, TA, WK,
834 CC, AM, KA and MB designed and produced the visualisations. HM prepared the original draft of the manuscript and
835 all co-authors were involved in the writing review and editing process.

836 **Competing Interests**

837 The authors declare that they have no conflict of interest.

838 **Acknowledgements**

839 This paper benefitted from discussion at events of the Past Global Changes (PAGES) working group ‘Volcanic
840 Impacts on Climate and Society’ (VICs), as well as with Angus M. Duncan and Richard J. Payne. PAGES is
841 supported by the Chinese Academy of Sciences (CAS), and Swiss Academy of Sciences (SCNAT). H. Mackay and
842 M. Amesbury were supported by the UK Natural Environment Research Council (PRECIP project grants
843 NE/G019851/1, NE/G020272/1, NE/G019673/1 and NE/G02006X/1 and MILLIPEAT project grant
844 NE/1012915/1). A Quaternary Research Association New Research Workers award granted to H. Mackay and the
845 NERC Radiocarbon Facility NRCF010001 (allocation numbers 1744.1013 and 1789.0414). C. Corona and M.
846 Stoffel were supported by the Swiss National Science Foundation Sinergia project CALDERA (grant agreement no.
847 CRSII5_183571). WMK and CCR are supported by the Swiss National Science Foundation (SNSF, grants
848 200020_172745 and 200020_200492). The climate mode simulations were performed at the Swiss National Super
849 Computing Centre (CSCS). M. Sigl acknowledges funding from the European Research Council (ERC) under the
850 European Union’s Horizon 2020 research and innovation program (grant agreement 820047). F. Ludlow and C.
851 Kostick were supported by an Irish Research Council Laureate Award (CLICAB, IRCLA/2017/303). J.G. Manning
852 and F. Ludlow also acknowledge support from US National Science Foundation Award # 1824770.



853 **References**

- 854 Abbott, P. M., Plunkett, G., Corona, C., Chellman, N. J., McConnell, J. R., Pilcher, J. R., Stoffel, M., and Sigl, M.:
855 Cryptotephra from the Icelandic Veidivötn 1477 CE eruption in a Greenland ice core: confirming the dating of
856 volcanic events in the 1450s CE and assessing the eruption's climatic impact, *Clim. Past*, 17, 565–585,
857 <https://doi.org/10.5194/cp-17-565-2021>, 2021.
- 858 Amesbury, M.J., Swindles, G.T., Bobrov, A., Charman, D.J., Holden, J., Lamentowicz, M., Mallon, G., Mazei, Y.,
859 Mitchell, E.A., Payne, R.J., and Roland, T.P.: Development of a new pan-European testate amoeba transfer function
860 for reconstructing peatland palaeohydrology, *Quaternary Sci. Rev.*, 152, 132–151,
861 <https://doi.org/10.1016/j.quascirev.2016.09.024>, 2016.
- 862 Amesbury, M.J., Booth, R.K., Roland, T.P., Bunbury, J., Clifford, M.J., Charman, D.J., Elliot, S., Finkelstein, S.,
863 Garneau, M., Hughes, P.D., and Lamarre, A.: Towards a Holarctic synthesis of peatland testate amoeba ecology:
864 Development of a new continental-scale palaeohydrological transfer function for North America and comparison to
865 European data, *Quaternary Sci. Rev.*, 201, 483–500, <https://doi.org/10.1016/j.quascirev.2018.10.034>, 2018.
- 866 Anchukaitis, K. J., Cook, E. R., Cook, B. I., Pearl, J., D'Arrigo, R., and Wilson, R.: Coupled modes of North
867 Atlantic ocean-atmosphere variability and the onset of the Little Ice Age, *Geophys. Res. Lett.*, 46, 12417–12426,
868 <https://doi.org/10.1029/2019GL084350>, 2019.
- 869 Aubry, T. J., Toohey, M., Marshall, L., Schmidt, A., and Jellinek, A. M.: A new volcanic stratospheric sulfate
870 aerosol forcing emulator (EVA_H): Comparison with interactive stratospheric aerosol models, *J. Geophys. Res. –*
871 *Atmos.*, 125, <https://doi.org/10.1029/2019JD031303>, 2020.
- 872 Aubry, T. J., Engwell, S., Bonadonna, C., Carazzo, G., Scollo, S., Van Eaton, A.R., Taylor, I.A., Jessop, D.,
873 Eychenne, J., Gouhier, M., Mastin, L. G., Wallace, K. L., Biass, S., Bursik, M., Grainger, R.G., Jellinek, A. M., and
874 Schmidt, A.: The Independent Volcanic Eruption Source Parameter Archive (IVESPA, version 1.0): A new
875 observational database to support explosive eruptive column model validation and development, *J. Volcanol. Geoth.*
876 *Res.*, 417, 107295, <https://doi.org/10.1016/j.jvolgeores.2021.107295>, 2021.
- 877 Bereiter, B., Eggleston, S., Schmitt, J., Nehrbass-Ahles, C., Stocker, T.F., Fischer, H., Kipfstuhl, S., and Chappellaz,
878 J.: Revision of the EPICA Dome C CO₂ record from 800 to 600 kyr before present, *Geophys. Res. Lett.*, 42, 542–
879 549, <https://doi.org/10.1002/2014GL061957>, 2015.
- 880 Berger, A.: Long-term variations of daily insolation and Quaternary climatic changes, *Journal of Atmospheric*
881 *Sciences*, 35, 2362–2367, [https://doi.org/10.1175/1520-0469\(1978\)035<2362:LTVODI>2.0.CO;2](https://doi.org/10.1175/1520-0469(1978)035<2362:LTVODI>2.0.CO;2), 1978.
- 882 Blaauw, M. and Christen, J. A.: Flexible paleoclimate age-depth models using an autoregressive gamma process,
883 *Bayesian Analysis*, 6, 457–474, <https://doi.org/10.1214/11-BA618>, 2011.



- 884 Blong, R., Fallon, S., Wood, R., McKee, C., Chen, K. P., Magill, C., and Barter, P.: Significance and timing of the
885 mid-17th-century eruption of Long Island, Papua New Guinea, *Holocene*, 28, 529-544,
886 <https://doi.org/10.1177/0959683617735589>, 2018.
- 887 Bonadonna, C. and Costa, A.: Estimating the volume of tephra deposits: a new simple strategy, *Geology*, 40, 415–
888 418, <https://doi.org/10.1130/G32769.1>, 2012.
- 889 Booth, R. K.: Testate amoebae as proxies for mean annual water-table depth in Sphagnum-dominated peatlands of
890 North America, *J. Quaternary Sci.*, 23, 43–57, <https://doi.org/10.1002/jqs.1114>, 2008.
- 891 Booth, R. K., Lamentowicz, M., and Charman, D. J.: Preparation and analysis of testate amoebae in peatland
892 palaeoenvironmental studies, *Mires & Peat*, 7, 2010.
- 893 Brenna, H., Kutterolf, S., Mills, M. J., and Krüger, K.: The potential impacts of a sulfur- and halogen-rich
894 supereruption such as Los Chocoyos on the atmosphere and climate, *Atmos. Chem. Phys.*, 20, 6521–6539,
895 <https://doi.org/10.5194/acp-20-6521-2020>, 2020.
- 896 Bunbury, J. and Gajewski, K.: Effects of the White River Ash event on aquatic environments, southwest Yukon,
897 Canada, *Arctic*, 17–31, <https://www.jstor.org/stable/23594603>, 2013.
- 898 Büntgen, U. and Tegel W.: European tree-ring data and the Medieval Climate Anomaly, *PAGES news*, 19,1, 14-15,
899 2011.
- 900 Büntgen, U., Myglan, C., Ljungqvist, F.: Cooling and societal change during the Late Antique Little Ice Age from
901 523 to around 660 AD, *Nat. Geosci.*, 9, 231-236, <https://doi.org/10.1038/ngeo2652>, 2016.
- 902 Büntgen, U., Asrenault, D., Boucher, E., Churakova (Sidorova), O.V., Gennaretti, F., Crivellaro, A., Hugher, M.K.,
903 Kirdvanov, A.V., Klippel, L., Krusic, P.J., Linerholm, H.W., Ljungqvist, F.D., Ludescher, J., McCormick, M., Sigl,
904 M., Vaganov, E.A. and Esper, J.: Prominent role of volcanism in Common Era climate variability and human
905 history, *Dendrochronologia*, 65, 125757, <https://doi.org/10.1016/j.dendro.2020.125757>, 2020.
- 906 Carey, S. and Sparks, R. S. J.: Quantitative models of the fallout and dispersal of tephra from volcanic eruption
907 columns, *Bull. Volcanol.*, 48, 109–125, <https://doi.org/10.1007/BF01046546>, 1986.
- 908 Charman, DJ, Hendon, D, Woodland, WA.: The identification of testate amoebae (Protozoa: Rhizopoda) in peats.
909 QRA Technical Guide No. 9. London: Quaternary Research Association. 147 pp, 2000.
- 910 Chen, Gaoyong et al. (ed.): *Zhongguo lidai tianzai renhuo biao* (Shanghai 1986), vol. 1, pp. 652-652, 1986.



- 911 Clifford, M.J. and Booth, R.K.: Increased probability of fire during late Holocene droughts in northern New
912 England, *Climatic change*, 119, 693–704, doi:10.1016/j.quaint.2011.05.027, 2013.
- 913 Cook, E. R., Meko, D. M., Stahle, D. W., and Cleaveland, M. K.: Drought reconstructions for the continental United
914 States. *Journal of Climate*, 12, 1145–1162, [https://doi.org/10.1175/1520-0442\(1999\)012<1145:DRFTCU>2.0.CO;2](https://doi.org/10.1175/1520-0442(1999)012<1145:DRFTCU>2.0.CO;2).
915 1999.
- 916 Cook, E. R., Seager, R., Heim Jr, R. R., Vose, R. S., Herweijer, C., and Woodhouse, C.: Megadroughts in North
917 America: placing IPCC projections of hydroclimatic change in a long-term palaeoclimate context. *J. Quaternary*
918 *Sci.*, 25, 48-61, <https://doi.org/10.1002/jqs.1303>, 2010.
- 919 Cook, E.R., Seager, R., Kushnir, Y., Briffa, K.R., Büntgen, U., Frank, D., Krusic, P.J., Tegel, W., van der Schrier,
920 G., Andreu-Hayles, L., Baillie, M., Baittinger, C., Bleicher, N., Bonde, N., Brown, D., Carrer, M., Cooper, R.,
921 Cufar, K., Dittmar, C., Esper, J., Griggs, C., Gunnarson, B., Gunther, B., Gutierrez, E., Haneca, K., Helama, S.,
922 Herzig, F., Heussner, K-U., Hofmann, J., Janda, P., Kontic, R., Kose, N., Kyncl, T., Levanic, T., Linderholm, H.,
923 Manning, S., Melvin, T. M., Miles, D., Neuwirth, B., Nicolussi, K., Nola, P., Panayotov, M., Popa, I., Rothe, A.,
924 Seftigen, K., Seim, A., Svarva, H., Svoboda, M., Thun, T., Timonen, M., Touchan, R., Trotsiuk, V., Trouet, V.,
925 Walder, F., Wazny, T., Wilson, R. and Zang, C.: Old World megadroughts and pluvials during the Common Era. *Sci*
926 *Adv*, 1, doi: 10.1126/sciadv.1500561, 2015.
- 927 Coulter, S. E., Pilcher, J. R., Plunkett, G., Baillie, M., Hall, V. A., Steffensen, J. P., Vinther, B. M., Clausen, H. B.,
928 and Johnsen, S. J.: Holocene tephras highlight complexity of volcanic signals in Greenland ice cores, *J. Geophys.*
929 *Res. – Atmos.*, 117, <https://doi.org/10.1029/2012JD017698>, 2012.
- 930 Coyle McClung, L.: A palynological investigation of land-use patterns in first millennium AD Ireland, unpublished
931 PhD thesis, Queen’s University Belfast, 2012.
- 932 Devroey, J.-P.: *La Nature et le Roi: Environnement, Pouvoir et Société à l’Âge de Charlemagne (740-820)*, Albin
933 Michel, Paris, 2019.
- 934 Duby, G.: *The Early Growth of the European Economy: Warriors and Peasants from the Seventh to the Twelfth*
935 *Century*, trans Clarke, H.B., Ithaca: Cornell Universty Press, 1974.
- 936 Fierstein, J. and Nathenson, M.: Another look at the calculation of fallout tephra volumes, *Bull. Volcanol.*, 54, 156–
937 167, <https://doi.org/10.1007/BF00278005>, 1992.
- 938 Guillet, S., Corona, C., Stoffel, M., Khodri, M., Lavigne, F., Ortega, P., Eckert, N., Seleniou, P., Daux, V.,
939 Churakova (Sidorova), O., Davi, N., Edouard, J.L., Yong, Z., Luckman, B.H., Myglan, V.S., Guiot, J., Beniston, M.,



- 940 Masson-Delmotte, V., Oppenheimer, C.: Climate response to the Samalas volcanic eruption in 1257 revealed by
941 proxy records. *Nature Geosci* 10, 123–128, <https://doi.org/10.1038/ngeo2875>, 2017.
- 942 Guillet, S., Corona, C., Ludlow, F., Oppenheimer, C., and Stoffel, M.: Climatic and societal impacts of a “forgotten”
943 cluster of volcanic eruptions in 1108–1110 CE, *Sci. Rep.*, 10, 1–10, <https://doi.org/10.1038/s41598-020-63339-3>,
944 2020.
- 945 Haldon, J., Mordechai, L., Newfield, T. P., Chase, A. F., Izdebski, A., Guzowski, P., Labuhn, I., and Roberts, N.:
946 History meets palaeoscience: Consilience and collaboration in studying past societal responses to environmental
947 change. *P. Natl. Acad. Sci. USA*, 115, 3210–3218, <https://doi.org/10.1073/pnas.1716912115>, 2018.
- 948 Hall, V. A.: The vegetation history of monastic and secular sites in the midlands of Ireland over the last two
949 millennia, *Vegetation History and Archaeobotany*, 15, 1–12, <https://doi.org/10.1007/s00334-005-0072-0>, 2005.
- 950 Hare, P.G., Greer, S., Gotthardt, R., Farnell, R., Bowyer, V., Schweger, C., and Strand, D.: Ethnographic and
951 archaeological investigations of alpine ice patches in southwest Yukon, Canada, *Arctic*, 260–272,
952 <https://www.jstor.org/stable/40512063>, 2004.
- 953 Hassan, F.A.: Extreme Nile floods and famines in Medieval Egypt (AD 930–1500) and their climatic implications,
954 *Quaternary International*, 173–174, 101–112, <https://doi.org/10.1016/j.quaint.2007.06.001>, 2007.
- 955 Hirsch, A.: *Handbook of Geographical and Historical Pathology*, vol. 2: Chronic Infective, Toxic, Parasitic, Septic
956 and Constitutional Diseases, trans. Charles Creighton, London: New Sydenham Society, 1885.
- 957 Held, I. M. and Soden, B. J.: Robust responses of the hydrological cycle to global warming. *J. Clim.* 19, 5686–5699,
958 <https://doi.org/10.1175/JCLI3990.1> 2006.
- 959 Hendon, D., and Charman, D.J.: The preparation of testate amoebae (Protozoa: Rhizopoda) samples from peat,
960 *Holocene*, 7, <https://doi.org/10.1177/095968369700700207>, 199–205, 1997.
- 961 Hogg, A., Lowe, D. J., Palmer, J., Boswijk, G., and Ramsey, C. B.: Revised calendar date for the Taupo eruption
962 derived by C-14 wiggle-matching using a New Zealand kauri C-14 calibration data set, *Holocene*, 22, 439–449,
963 <https://doi.org/10.1177/0959683611425551>, 2012.
- 964 Hogg, A. G., Wilson, C. J. N., Lowe, D. J., Turney, C. S. M., White, P., Lorrey, A. M., Manning, S. W., Palmer, J.
965 G., Bury, S., Brown, J., Southon, J., and Petchey, F.: Wiggle-match radiocarbon dating of the Taupo eruption, *Nat*
966 *Commun*, 10, <https://doi.org/10.1038/s41467-019-12532-8>, 2019.
- 967 Hurrell, J. W., Holland, M. M., Gent, P. R., Ghan, S., Kay, J. E., Kushner, P. J., Lamarque, J. F., Large, W. G.,
968 Lawrence, D., Lindsay, K., and Lipscomb, W. H.: The community earth system model: a framework for



- 969 collaborative research, *Bulletin of the American Meteorological Society*, 94, 1339–1360,
970 <https://doi.org/10.1175/BAMS-D-12-00121.1>, 2013.
- 971 Iles, C.E. and Hegerl, G. C.: The global precipitation response to volcanic eruptions in the CMIP5 models,
972 *Environmental Research Letters*, 9, 104012, <https://doi.org/10.1088/1748-9326/9/10/104012>, 2014.
- 973 Iles, C. and Hegerl, G.C.: Systematic change in global patterns of streamflow following volcanic eruptions. *Nature*
974 *Geosci.*, 8, 838–842, <https://doi.org/10.1038/ngeo2545>, 2015.
- 975 Jensen, B. J., Pyne-O’Donnell, S., Plunkett, G., Froese, D. G., Hughes, P. D., Sigl, M., McConnell, J. R., Amesbury,
976 M. J., Blackwell, P. G., van den Bogaard, C., Buck, C. E., Charman, D.J., Clague, J. J., Hall, V. A., Koch, J.,
977 Mackay, H., Mallon, G., McColl, L., and Pilcher, J. R.: Transatlantic distribution of the Alaskan White River Ash,
978 *Geology* 42, <https://doi.org/10.1130/G35945.1>, 875–878, 2014.
- 979 Jensen, B. J. L., Davies, L. D., Nolan, C., Pyne-O’Donnell, S., Monteath, A. J., Ponomareva, V., Portnyagin, M.,
980 Booth, R., Bursik, M., Cook, E., Plunkett, G., Vallance, J. W., Luo, Y., Cwynar, L. C., Hughes, P., and Pearson, G.
981 D.: A latest Pleistocene and Holocene composite tephrostratigraphic framework for northeastern North America,
982 *Quaternary Sci. Rev.*, in press 2021.
- 983 Joos, F. and Spahni, R.: Rates of change in natural and anthropogenic radiative forcing over the past 20,000 years, P.
984 *Natl. Acad. Sci. USA*, 105, 1425–1430, <https://doi.org/10.1073/pnas.0707386105>, 2008.
- 985 Jungclaus, J. H., Bard, E., Baroni, M., Braconnot, P., Cao, J., Chini, L. P., Egorova, T., Evans, M., González-Rouco,
986 J. F., Goosse, H., and Hurr, G. C.: The PMIP4 contribution to CMIP6–Part 3: The last millennium, scientific
987 objective, and experimental design for the PMIP4 past1000 simulations, *Geoscientific Model Development*, 10,
988 4005–4033, <https://doi.org/10.5194/gmd-10-4005-2017>, 2017.
- 989 Kageyama, M., Braconnot, P., Harrison, S. P., Haywood, A. M., Jungclaus, J. H., Otto-Bliesner, B. L., Peterschmitt,
990 J. Y., Abe-Ouchi, A., Albani, S., Bartlein, P. J., and Brierley, C.: The PMIP4 contribution to CMIP6–Part 1:
991 Overview and over-arching analysis plan, *Geoscientific Model Development*, 11, 1033–1057,
992 <https://doi.org/10.5194/gmd-11-1033-2018>, 2018.
- 993 Kerr, T. R., Swindles, G. T., and Plunkett, G.: Making hay while the sun shines? Socio-economic change, cereal
994 production and climatic deterioration in Early Medieval Ireland, *Journal of Archaeological Science*, 36, 2868–2874,
995 <https://doi.org/10.1016/j.jas.2009.09.015>, 2009.
- 996 Kim, W. M., Blender, R., Sigl, M., Messmer, M., and Raible, C. C.: Statistical characteristics of extreme daily
997 precipitation during 1501 BCE–1849 CE in the Community Earth System Model. *Climate of the Past*, 17(5), 2031–
998 2053, <https://doi.org/10.5194/cp-17-2031-2021>, 2021.



- 999 Kinder, M., Wulf, S., Appelt, O., Hardiman, M., Żarczyński, M., and Tylmann, W.: Late-Holocene ultra-distal
1000 cryptotephra discoveries in varved sediments of Lake Żabińskie, NE Poland, *J. Volcanol. Geoth. Res.*, 402, 106988,
1001 <https://doi.org/10.1016/j.jvolgeores.2020.106988>, 2020.
- 1002 Kodisch, A., Wilde, P., Schmiedchen, B., Fromme, F.-J., Rodemann, B., Tratwal, A., Oberforster, M., Wieser, F.,
1003 Schiermann, A., Jorgensen, L.N. and Miedaner, T.: Ergot infection in winter rye hybrids shows differential
1004 contribution of male and female genotypes and environment, *Euphytica* 216, 65, [https://doi.org/10.1007/s10681-](https://doi.org/10.1007/s10681-020-02600-2)
1005 020-02600-2, 2020.
- 1006 Kondrashov, D., Feliks, Y., and Ghil, M.: Oscillatory modes of extended Nile River records (A.D. 622–1922),
1007 *Geophys. Res. Lett.*, 32, L10702, doi:10.1029/2004GL022156, 2005.
- 1008 Kristensen, T. J., Beaudoin, A. B., and Ives, J. W.: Environmental and Hunter-Gatherer Responses to the White
1009 River Ash East Volcanic Eruption in the Late Holocene Canadian Subarctic, *Arctic*, 73, 153–186, 2020.
- 1010 Ladd, M., Viau, A.E., Way, R.G., Gajewski, K. and Sawada, M.C.: Variations in precipitation in North America
1011 during the past 2000 years, *The Holocene* 28, 4, 667–675. <https://doi.org/10.1177/0959683617735583>, 2018.
- 1012 Lerbekmo, J. F., Westgate, J. A., Smith, D. G. W., and Denton, G. H.: New data on the character and history of the
1013 White River volcanic eruption, Alaska, in: *Quaternary studies*, edited by Suggate, R.P. and Cresswell, M.M.,
1014 Wellington, Royal Society of New Zealand, 203–209, 1975.
- 1015 Lerbekmo, J. F.: The White river ash: largest Holocene Plinian tephra, *Canadian Journal of Earth Sciences* 45, 693–
1016 700, <https://doi.org/10.1139/E08-023>, 2008.
- 1017 Ludlow, F.: The utility of the Irish Annals as a source for the reconstruction of the climate. Unpublished PhD thesis,
1018 Trinity College Dublin, 2010.
- 1019 Ludlow, F., Stine, A.R., Leahy, P., Murphy, E., Mayewski, P.A., Taylor, D., Killen, J., Baillie, M.G.L., Hennessy,
1020 M and Kiely, G.: Medieval Irish chronicles reveal persistent volcanic forcing of severe winter cold events, 431–1649
1021 CE. *Environmental Research Letters*. 8, 2, 024035. <https://doi.org/10.1088/1748-9326/8/2/024035>, 2013
- 1022 Mackay, H., Hughes, P. D. M., Jensen, B. J. L., Langdon, P. G., Pyne-O'Donnell, S., Plunkett, G., Froese, D. G.,
1023 and Coulter, S.: The foundations of a late Holocene tephrostratigraphic framework for eastern North America,
1024 *Quaternary Sci. Rev.* 132, 101–113, <https://doi.org/10.1016/j.quascirev.2015.11.011>, 2016.
- 1025 Mackay, H., Amesbury, M. J., Langdon, P. G., Charman, D. J., Magnan, G., van Bellen, S., Garneau, M.,
1026 Bainbridge, R., and Hughes, P. D.: Spatial variation of hydroclimate in north-eastern North America during the last
1027 millennium, *Quaternary Sci. Rev.*, 256, 106813, <https://doi.org/10.1016/j.quascirev.2021.106813>, 2021.



- 1028 Maeno, F., Nakada, S., Yoshimoto, M., Shimano, T., Hokanishi, N., Zaennudin, A., and Iguchi, M.: A sequence of a
1029 plinian eruption preceded by dome destruction at Kelud volcano, Indonesia, on February 13, 2014, revealed from
1030 tephra fallout and pyroclastic density current deposits, *J. Volcanol. Geoth. Res.*, 382, 24–41,
1031 <https://doi.org/10.1016/j.jvolgeores.2017.03.002>, 2019.
- 1032 Mann, M.E., Zhang, Z., Hughes, M.K., Bradley, R.S., Miller, S.K., Rutherford, S., and Ni, F.: Proxy-based
1033 reconstructions of hemispheric and global surface temperature variations over the past two millennia, *P. Natl. Acad.*
1034 *Sci. USA*, 105, 13252–13257. <https://doi.org/10.1073/pnas.0805721105>, 2008.
- 1035 Mann, M.E., Zhang, Z., Rutherford, S., Bradley, R.S., Hughes, M.K., Shindell, D., Ammann, C., Faluvegi, G., and
1036 Ni, F.: Global signatures and dynamical origins of the Little Ice Age and Medieval Climate Anomaly, *Science*, 326,
1037 1256–1260. DOI: 10.1126/science.1177303, 2009.
- 1038 Manning, J.G., Ludlow, F., Stine, A.R., Boos, W.R., Sigl, M. and Marlon, J.R.: Volcanic suppression of Nile
1039 summer flooding triggers revolt and constrains interstate conflict in ancient Egypt. *Nat. Commun.* 8, 900,
1040 <https://doi.org/10.1038/s41467-017-00957-y>, 2017.
- 1041 Marlon, J.R., Pederson, N., Nolan, C., Goring, S., Shuman, B., Robertson, A., Booth, R., Bartlein, P.J., Berke, M.A.,
1042 Clifford, M., Cook, E., Dieffenbacher-Krall, A., Dietze, M.C., Hessl, A., Hubeny, J.B., Jackson, S.T., Marsicek, J.,
1043 McLachlan, J., Mock, C.J., Moore, D.J.P., Nichols, J.Peteet, D., Schaefer, K., Trouet, V., Umbanhowar, C.,
1044 Williams, J.W. and Yu, Z.: Climatic history of the northeastern United States during the past 3000 years. *Clim.*
1045 *Past*, 13, 1355-1379, doi:10.5194/cp-13-1355-2017, 2017.
- 1046 Marshall, L., Johnson, J.S., Mann, G.W., Lee, L., Dhomse, S.S., Regayre, L., Yoshioka, M., Carslaw, K.S., and
1047 Schmidt, A.: Exploring how eruption source parameters affect volcanic radiative forcing using statistical emulation,
1048 *J. Geophys. Res. – Atmos.*, 124, 964–985. <https://doi.org/10.1029/2018JD028675>, 2019.
- 1049 Marshall, L.R., Smith, C.J., Forster, P.M., Aubry, T.J., Andrews, T., and Schmidt, A.: Large variations in volcanic
1050 aerosol forcing efficiency due to eruption source parameters and rapid adjustments, *Geophys. Res. Lett.*, 47,
1051 p.e2020GL090241. <https://doi.org/10.1029/2020GL090241>, 2020.
- 1052 McCarthy D. and Breen A.: An evaluation of astronomical observations in the Irish annals, *Vistas Astron.*, 41, 117–
1053 38, [https://doi.org/10.1016/S0083-6656\(96\)00052-9](https://doi.org/10.1016/S0083-6656(96)00052-9), 1997.
- 1054 McCarthy, D.: *The Irish Annals: their genesis, evolution and history*. Dublin: Four Courts Press,
1055 <https://doi.org/10.1017/S0021121400005940>, 2008.
- 1056 McConnell, J.R., Sigl, M., Plunkett, G., Burke, A., Kim, W.M., Raible, C.C., Wilson, A.I., Manning, J.G., Ludlow,
1057 F., Chellman, N.J., and Innes, H.M.: Extreme climate after massive eruption of Alaska’s Okmok volcano in 43 BCE



- 1058 and effects on the late Roman Republic and Ptolemaic Kingdom, *P. Natl. Acad. Sci. USA*, 117, 15443–15449.
1059 <https://doi.org/10.1073/pnas.2002722117>, 2020.
- 1060 McLaughlin, T. R.: An archaeology of Ireland for the Information Age, *Emania*, 25, 7–29, 2020.
- 1061 McLaughlin, R., Hannah, E., and Coyle-McClung, L.: Frequency analyses of historical and archaeological datasets
1062 reveal the same pattern of declining sociocultural activity in 9th to 10th century CE Ireland, *Clodynamics*, 9, 1,
1063 <https://doi.org/10.21237/C7clio9136654>, 2018.
- 1064 Meklach Y., Camenisch C., Merzouki A., García-Herrera R.: Potential of Arabic documentary sources for
1065 reconstructing past climate in the western Mediterranean region from AD 680 to 1815, *The Holocene*, 31, 11-12,
1066 1662-1669, [10.1177/09596836211033202](https://doi.org/10.1177/09596836211033202), 2021.
- 1067 Mitchell, E.A., Charman, D.J., and Warner, B.G.: Testate amoebae analysis in ecological and paleoecological
1068 studies of wetlands: past, present and future, *Biodiversity and conservation*, 17, 2115–2137,
1069 <https://doi.org/10.1007/s10531-007-9221-3>, 2008.
- 1070 Monteath, A. J., Teuten, A. E., Hughes, P. D. M., and Wastegård, S.: The effects of the peat acid digestion protocol
1071 on geochemically and morphologically diverse tephra deposits, *J. Quaternary Sci.* 34, 269–274,
1072 <https://doi.org/10.1002/jqs.3104>, 2019.
- 1073 Muhs, D. R., and Budahn, J. R.: Geochemical evidence for the origin of late Quaternary loess in central Alaska,
1074 *Canadian Journal of Earth Sciences*, 43, 323–337, <https://doi.org/10.1139/e05-115>, 2006.
- 1075 Mullen, P. O.: An archaeological test of the effects of the White River Ash eruptions, *Arctic Anthropology*, 49, 35–
1076 44, doi: [10.1353/arc.2012.0013](https://doi.org/10.1353/arc.2012.0013), 2012.
- 1077 Neukom, R., Steiger, N., Gómez-Navarro, J.J., Wang, J. and Werner, J.P.: No evidence for globally coherent warm
1078 and cold periods over the preindustrial Common Era, *Nature*, 571, 550–554, [https://doi.org/10.1038/s41586-019-](https://doi.org/10.1038/s41586-019-1401-2)
1079 1401-2, 2019.
- 1080 Newfield, T.: The contours of disease and hunger in Carolingian and early Ottonian Europe (c.750-c.950 CE),
1081 Unpublished PhD Thesis, McGill University, 2010.
- 1082 Newfield, T.: “The Contours, Frequency and Causation of Subsistence Crises in Carolingian Europe (750-950)” in
1083 P. Benito i Monclús ed., *Crisis Alimentarias en la Edad Media: Modelos, Explicaciones y Representaciones* (Lleida,
1084 2013), pp. 117-172. 2013.



- 1085 Oman, L., Robock, A., Stenchikov, G.L. and Thordarson, T.: High-latitude eruptions cast shadow over the African
1086 monsoon and the flow of the Nile, *Geophysical Research Letters*, 33, 18, <https://doi.org/10.1029/2006GL027665>,
1087 2006.
- 1088 Oppenheimer, C., Wacker, L., Xu, J., Galvan, J. D., Stoffel, M., Guillet, S., Corona, C., Sigl, M., Di Cosmo, N.,
1089 Hajdas, I., Pan, B., Breuker, R., Schneider, L., Esper, J., Fei, J., Hammond, J. O. S., and Büntgen, U.: Multi-proxy
1090 dating the ‘Millennium Eruption’ of Changbaishan to late 946 CE, *Quaternary Sci Rev*, 158, 164–171,
1091 <https://doi.org/10.1016/j.quascirev.2016.12.024>. 2017.
- 1092 Oppenheimer, C., Orchard, A., Stoffel, M., Newfield, T.P., Guillet, S., Corona, C., Sigl, M., Di Cosmo, N., and
1093 Büntgen, U.: The Eldgjá eruption: timing, long-range impacts and influence on the Christianisation of Iceland.
1094 *Climatic Change* 147, 369–381, <https://doi.org/10.1007/s10584-018-2171-9>, 2018.
- 1095 Patterson, R. T., Crann, C. A., Cutts, J. A., Mustaphi, C. J. C., Nasser, N. A., Macumber, A. L., Galloway, J. M.,
1096 Swindles, G. T., and Falck, H.: New occurrences of the White River Ash (east lobe) in Subarctic Canada and utility
1097 for estimating freshwater reservoir effect in lake sediment archives, *Palaeogeography, Palaeoclimatology,*
1098 *Palaeoecology*, 477, 1–9, <https://doi.org/10.1016/j.palaeo.2017.03.031>, 2017.
- 1099 Payne, R. and Blackford, J.: Distal volcanic impacts on peatlands: palaeoecological evidence from Alaska,
1100 *Quaternary Sci. Rev.*, 27, 2012–2030, <https://doi.org/10.1016/j.quascirev.2008.08.002>, 2008.
- 1101 Payne, R. J., and Mitchell, E. A.: How many is enough? Determining optimal count totals for ecological and
1102 palaeoecological studies of testate amoebae, *J. Paleolim.*, 42, 483–495, <https://doi.org/10.1007/s10933-008-9299-y>,
1103 2009.
- 1104 Pilcher, J. R., Hall, V. A., and McCormac, F. G.: An outline tephrochronology for the Holocene of the north of
1105 Ireland, *J. Quat. Sci.*, 11, 485–494 [https://doi.org/10.1002/\(SICI\)1099-1417\(199611/12\)11:6<485::AID-
1106 JQS266>3.0.CO;2-T](https://doi.org/10.1002/(SICI)1099-1417(199611/12)11:6<485::AID-JQS266>3.0.CO;2-T), 1996.
- 1107 Pyle, D.M.: The thickness, volume and grainsize of tephra fall deposits, *Bull. Volcanol.*, 51, 1–15,
1108 <https://doi.org/10.1007/BF01086757>, 1989.
- 1109 Pyne O’Donnell, S.D.F., Hughes, P.D.M., Froese, D.G., Jensen, B.J.L., Kuehn, S.C., Mallon, G., Amesbury, M.J.,
1110 Charman, D.J., Daley, T.J., Loader, N.J., Mauquoy, D., Street-Perrott, F.A., and Woodman-Ralph, J.: High-
1111 precision ultra-distal Holocene tephrochronology in North America. *Quat. Sci. Rev.* 52, 6–11,
1112 <https://doi.org/10.1016/j.quascirev.2012.07.024>, 2012.



- 1113 Rainville, R. A.: Effects of the White River and Mazama tephra on terrestrial and aquatic palaeoenvironments in
1114 western Subarctic Canada, and implications for past human populations, Doctoral dissertation, University of
1115 Calgary, 2016.
- 1116 Reimer, P.J., Austin, W.E.N., Bard, E., Bayliss, A., Blackwell, P.G., Bronk Ramsey, C., Butzin, M., Cheng, H.,
1117 Edwards, R.L., Friedrich, M., Grootes, P.M., Guilderson, T.P., Hajdas, I., Heaton, T.J., Hogg, A.G., Hughen, K.A.,
1118 Kromer, B., Manning, S.W., Muscheler, R., Palmer, J.G., Pearson, C., van der Plicht, J., Reimer, R.W., Richards,
1119 D.A., Scott, E.M., Southon, J.R., Turney, C.S.M., Wacker, L., Adolphi, F., Büntgen, U., Capano, M., Fahrni, S.M.,
1120 Fogtmann-Schulz, A., Friedrich, R., Kohler, P., Kudsk, S., Miyake, F., Olsen, J., Reinig, F., Sakamoto, M.,
1121 Sookdeo, A. and Talamo, S.: The IntCal20 northern hemisphere radiocarbon age calibration curve (0-55 cal kBP),
1122 *Radiocarbon*, 62, 4, 725-757, doi:10.1017/RDC.2020.41, 2020.
- 1123 Richter, D.H., Preece, S.J., McGimsey, R.G., and Westgate, J.A.: Mount Churchill, Alaska: The source of the late
1124 Holocene White River Ash: *Canadian Journal of Earth Sciences*, v. 32, p. 741–748, doi:10.1139/e95-063, 1995.
- 1125 Robock, A. and Liu, Y.: The volcanic signal in Goddard Institute for Space Studies three-dimensional model
1126 simulations, *J. Climate*, 7, 44–55, [https://doi.org/10.1175/1520-0442\(1994\)007<0044:TVSIGI>2.0.CO;2](https://doi.org/10.1175/1520-0442(1994)007<0044:TVSIGI>2.0.CO;2), 1994
- 1127 Schmidt, A., Mills, M. J., Ghan, S., Gregory, J. M., Allan, R. P., Andrews, T., Bardeen, C. G., Conley, A., Forster,
1128 P. M., Gettelman, A., and Portmann, R. W.: Volcanic radiative forcing from 1979 to 2015, *J. Geophys. Res. –*
1129 *Atmos.*, 123, 12491–12508, <https://doi.org/10.1029/2018JD028776>, 2018.
- 1130 Schneider, T., Bischoff, T., and Plotka, H.: Physics of changes in synoptic midlatitude temperature variability, *J.*
1131 *Climate*, 28, 2312–2331, <https://doi.org/10.1175/JCLI-D-14-00632.1>, 2015.
- 1132 Shuman, N.N., Routson, C., McKay, N., Fritz, S., Kaufman, D., Kirby, M.E., Nolar, C., Pederson, G.T. and St-
1133 Jacques, J.-M.: Placing the Common Era in a Holocene context: millennial to centennial patterns and trends in the
1134 hydroclimate of North America over the past 2000 years, *Clim. Past*, 14, 665-686, [https://doi.org/10.5194/cp-14-](https://doi.org/10.5194/cp-14-665-2018)
1135 665-2018, 2018.
- 1136 Sigl, M., McConnell, J.R., Layman, L., Maselli, O., McGwire, K., Pasteris, D., Dahl-Jensen, D., Steffensen, J.P.,
1137 Vinther, B., Edwards, R., and Mulvaney, R.: A new bipolar ice core record of volcanism from WAIS Divide and
1138 NEEM and implications for climate forcing of the last 2000 years, *J. Geophys. Res. – Atmos.*, 118, 1151–1169,
1139 <https://doi.org/10.1029/2012JD018603>, 2013.
- 1140 Sigl, M., McConnell, J. R., Toohey, M., Curran, M., Das, S. B., Edwards, R., Isaksson, E., Kawamura, K.,
1141 Kipfstuhl, S., Kruger, K., Layman, L., Maselli, O. J., Motizuki, Y., Motoyama, H., Pasteris, D. R., and Severi, M.:
1142 Insights from Antarctica on volcanic forcing during the Common Era, *Nat. Clim. Change*, 4, 693–697,
1143 <https://doi.org/10.1038/nclimate2293>, 2014.



- 1144 Sigl, M., Winstrup, M., McConnell, J. R., Welten, K. C., Plunkett, G., Ludlow, F., Büntgen, U., Caffee, M.,
1145 Chellman, N., Dahl-Jensen, D., Fischer, H., Kipfstuhl, S., Kostick, C., Maselli, O. J., Mekhaldi, F., Mulvaney, R.,
1146 Muscheler, R., Pasteris, D. R., Pilcher, J. R., Salzer, M., Schupbach, S., Steffensen, J. P., Vinther, B. M., and
1147 Woodruff, T. E.: Timing and climate forcing of volcanic eruptions for the past 2,500 years, *Nature*, 523, 543–549,
1148 <https://doi.org/10.1038/nature14565>, 2015.
- 1149 Sigl, M., Toohey, M., McConnell, J. R., Cole-Dai, J., Severi, M.: HolVol: Reconstructed volcanic stratospheric
1150 sulfur injections and aerosol optical depth for the Holocene (9500 BCE to 1900 CE).
1151 PANGAEA, <https://doi.org/10.1594/PANGAEA.928646>, 2021.
- 1152 Somers, Robert M.: “The End of the T’ang” in *The Cambridge History of China. Volume 3: Sui and T’ang China*,
1153 589–906 AD, Part One. Ed Denis Twitchett (Cambridge 1979), p. 696. 1979.
- 1154 Staunton-Sykes, J., Aubry, T. J., Shin, Y. M., Weber, J., Marshall, L. R., Luke Abraham, N., Archibald, A., and
1155 Schmidt, A.: Co-emission of volcanic sulfur and halogens amplifies volcanic effective radiative forcing,
1156 *Atmospheric Chemistry and Physics*, 21, 9009–9029, <https://doi.org/10.5194/acp-2020-1110>, 2021.
- 1157 Stoffel, M., Khodri, M., Corona, C., Guillet, S., Poulain, V., Bekki, S., Guiot, J., Luckman, B.H., Oppenheimer, C.,
1158 Lebas, N., Beniston, M., Masson-Delmotte, V.: Estimates of volcanic-induced cooling in the Northern Hemisphere
1159 over the past 1,500 years. *Nature Geosci* 8, 784–788 (2015). <https://doi.org/10.1038/ngeo2526>, 2015.
- 1160 Sun, C., Plunkett, G., Liu, J., Zhao, H., Sigl, M., McConnell, J. R., Pilcher, J. R., Vinther, B., Steffensen, J. P., and
1161 Hall, V.: Ash from Changbaishan Millennium eruption recorded in Greenland ice: Implications for determining the
1162 eruption’s timing and impact, *Geophys. Res. Lett.*, 41, 694–701, <https://doi.org/10.1002/2013GL058642>, 2014.
- 1163 Swindles, G.T., Blundell, A., Roe, H.M., and Hall, V.A.: A 4500-year proxy climate record from peatlands in the
1164 North of Ireland: the identification of widespread summer ‘drought phases’?, *Quaternary Science Reviews*, 29, 13–
1165 14, <https://doi.org/10.1016/j.quascirev.2009.01.003>, 2010.
- 1166 Swindles, G.T., Morris, P.J., Baird, A.J., Blaauw, M., Plunkett, G.: Ecohydrological feedbacks confound peat-based
1167 climate reconstructions, *Geophysical Research Letters*, 39, 11, <https://doi.org/10.1029/2012GL051500>, 2012.
- 1168 Swindles, G. T., Holden, J., Raby, C. L., Turner, T. E., Blundell, A., Charman, D. J., Menberu, M. W., and Kløve,
1169 B.: Testing peatland water-table depth transfer functions using high-resolution hydrological monitoring data,
1170 *Quaternary Sci. Rev.*, 120, 107–117. <https://doi.org/10.1016/j.quascirev.2015.04.019>, 2015.
- 1171 Thomason, L. W., Ernest, N., Millán, L., Rieger, L., Bourassa, A., Vernier, J. P., Manney, G., Luo, B., Arfeuille, F.,
1172 and Peter, T.: A global space-based stratospheric aerosol climatology: 1979–2016, *Earth System Science Data*, 10,
1173 469–492, <https://doi.org/10.5194/essd-10-469-2018>, 2018.



- 1174 Timmerck, C., Toohey, M., Zanchettin, D., Bronnimann, S., Lundstad, E. and Wilson, R.: The unidentified eruption
1175 of 1809: a climatic cold case. *Clim. Past*, 17, 1455-1482, <https://doi.org/10.5194/cp-17-1455-2021>, 2021.
- 1176 Toohey, M., and Sigl, M.: Volcanic stratospheric sulfur injections and aerosol optical depth from 500 BCE to 1900
1177 CE, *Earth System Science Data*, 9, 809–831, <https://doi.org/10.5194/essd-9-809-2017>, 2017.
- 1178 Toohey, M., Stevens, B., Schmidt, H., and Timmreck, C.: Easy Volcanic Aerosol (EVA v1. 0): an idealized forcing
1179 generator for climate simulations, *Geoscientific Model Development*, 9, 4049–4070, <https://doi.org/10.5194/gmd-9-4049-2016>, 2016.
- 1181 Toohey, M., Krüger, K., Schmidt, H., Timmreck, C., Sigl, M., Stoffel, M., and Wilson, R.: Disproportionately
1182 strong climate forcing from extratropical explosive volcanic eruptions, *Nature Geoscience*, 12, 100–107,
1183 https://doi.org/10.1594/WDC/eVol2k_v2, 2019.
- 1184 Usoskin, I.G., Hulot, G., Gallet, Y., Roth, R., Licht, A., Joos, F., Kovaltsov, G.A., Thébault, E., and Khokhlov, A.:
1185 Evidence for distinct modes of solar activity, *Astronomy & Astrophysics*, 562, p.L10, <https://doi.org/10.1051/0004-6361/201423391>, 2014.
- 1187 Usoskin, I.G., Gallet, Y., Lopes, F., Kovaltsov, G.A., and Hulot, G.: Solar activity during the Holocene: the Hallstatt
1188 cycle and its consequence for grand minima and maxima, *Astronomy & Astrophysics*, 587, A150,
1189 <https://doi.org/10.1051/0004-6361/201527295>, 2016.
- 1190 Vernier, J.-P., Fairlie, T. D., Deshler, T., Natarajan, M., Knepp, T., Foster, K., Wienhold, F. G., Bedka, K. M.,
1191 Thomason, L., and Trepte, C.: In situ and space-based observations of the Kelud volcanic plume: The persistence of
1192 ash in the lower stratosphere, *J. Geophys. Res. Atmos.*, 121, 11,104– 11,118, doi:10.1002/2016JD025344, 2016.
- 1193 Vieira, L. E. A., Solanki, S. K., Krivova, N. A., and Usoskin, I.: Evolution of the solar irradiance during the
1194 Holocene, *Astronomy & Astrophysics*, 531, A6, <https://doi.org/10.1051/0004-6361/201015843>, 2011.
- 1195 Vinther, B. M., Clausen, H. B., Johnsen, S. J., Rasmussen, S. O., Andersen, K. K., Buchardt, S. L., Dahl-Jensen, D.,
1196 Seierstad, I. K., Siggaard-Andersen, M.-L., Steffensen, J. P., Svensson, A., Olsen, J., and Heinemeier, J.: A
1197 synchronized dating of three Greenland ice cores throughout the Holocene, *J. Geophys. Res.*, 111, D13102,
1198 <https://doi.org/10.1029/2005JD006921>, 2006.
- 1199 Wade, D. C., Vidal, C. M., Abraham, N. L., Dhomse, S., Griffiths, P. T., Keeble, J., Mann, G., Marshall, L.,
1200 Schmidt, A., and Archibald, A.T.: Reconciling the climate and ozone response to the 1257 CE Mount Samalas
1201 eruption. *P. Natl. Acad. Sci. USA*, 117, 26651–26659, <https://doi.org/10.1073/pnas.1919807117>, 2020.



- 1202 Watson, E.J., Kołaczek, P., Słowiński, M., Swindles, G.T., Marcisz, K., Galka, M., and Lamentowicz, M.: First
1203 discovery of Holocene Alaskan and Icelandic tephra in Polish peatlands, *J. Quaternary Sci.* 32, 457–462, DOI:
1204 10.1002/jqs.2945, 2017a.
- 1205 Watson, E. J., Swindles, G. T., Lawson, I. T., Savov, I. P., and Wastegård, S.: The presence of Holocene
1206 cryptotephra in Wales and southern England, *J. Quaternary Sci.*, 32, 493–500, /doi/pdf/10.1002/jqs.2942, 2017b.
- 1207 West, K. D. and Donaldson, J. A.: Evidence for winter eruption of the White River Ash (eastern lobe), Yukon
1208 Territory, Canada, *Geocanada 2000 – The Millennium Geoscience Summit, Conference CD*, 2000.
- 1209 White, S., Moreno-Chamarro, E., Zanchettin, D., Huhtamaa, H., Degroot, D., Stoffel, M., and Corona, C.: The 1600
1210 Huaynaputina Eruption as Possible Trigger for Persistent Cooling in the North Atlantic Region, *Clim. Past Discuss.*
1211 [preprint], <https://doi.org/10.5194/cp-2021-82>, in review, 2021.
- 1212 Wilson, R., Anchukaitis, K., Briffa, K.R., Büntgen, U., Cook, E., D’Arrigo, R., Davi. N., Esper, J., Frank, D.,
1213 Gunnarson, B., Hegerl, G., Helama, D., Klesse, S., Krusic, P.J., Linderholm, H.W., Myglan, V., Osborn, T.J.,
1214 Rydval, M., Schneider, L., Schurer, A., Wiles, G., Zhang, P. and Zorita, E.: Last millennium northern hemisphere
1215 summer temperatures from tree rings: Part 1: The long term context, *Quaternary Science Reviews*, 138, 1-18,
1216 10.1016/j.quascirev.2015.12.005, 2016.
- 1217 Woodland, W. A., Charman, D. J., and Sims, P. C.: Quantitative estimates of water tables and soil moisture in
1218 Holocene peatlands from testate amoebae, *Holocene*, 8, 261–273, <https://doi.org/10.1191/095968398667004497>,
1219 1998.
- 1220 Yin, S., Huang, C., and Li, X.: Historical drought and water disasters in the Weihe Plain, *J. Geogr. Sci.* 15, 97–105,
1221 <https://doi.org/10.1007/BF02873112>, 2005.
- 1222 Zhang, De’er, *Zhongguo san qian nian qi xiang ji lu zong ji* (Nanjing 2004), v. 1, pp. 363-364. 2004.
- 1223 Zhu, Y., Toon, O.B., Jensen, E.J., Bardeen, C.G., Mills, M.J., Tolbert, M.A., Yu, P., and Woods, S.: Persisting
1224 volcanic ash particles impact stratospheric SO₂ lifetime and aerosol optical properties, *Nat. Commun.*, 11, 4526.
1225 <https://doi.org/10.1038/s41467-020-18352-5>, 2020.
- 1226 Zhuo, Z., Gao, C. and Pan, Y.: Proxy evidence for China’s monsoon precipitation response to volcanic aerosols over
1227 the past seven centuries, *J. Geophys. Res. Atmos.*, 119, 6638–6652, <https://doi.org/10.1002/2013JD021061>, 2014.